ABSTRACT

AGGARWAL, SACHIN. An Inviscid Numerical Method for Unsteady Flows over Airfoils and Wings to Predict the Onset of Leading Edge Vortex Formation. (Under the direction of Dr. Ashok Gopalarathnam.)

A numerical method based on distribution of discrete vortex elements for unsteady motions of two-dimensional airfoils and three-dimensional wings is developed. The main objective was to determine the onset criterion for formation of leading edge vortices. The objective of this research effort is to find a parameter in the numerical model that is similar to the leading edge suction parameter (LESP) that has been developed in recent theoretical work and compare the results from this numerical model with the previously-developed theoretical model, computations and experiments. It is shown that the strength of the forward-most discrete bound vortex has a behavior that is very similar to the LESP, and can be used as a proxy for the LESP. Results from this model are shown to match with those from the theoretical model and for a range of pitch and plunge motions. Thus the numerical model can be used instead of the theoretical model to study unsteady motions and predict the onset of LEV formation during these motions. The advantage of the numerical model is that it can be easily extended to three-dimensional wings and rotor shapes. An extension to the LESP criterion to three-dimensional wing and rotor analysis using unsteady vortex lattice method is carried out. Results from this extended model are shown to be a very good match with results in the literature for some steady and unsteady motions. The numerical method was also used to study two pitching motions for a finite wing of aspect ratio 2, with pivot points at the quarter-chord and three quarter-chord locations. In both cases, comparison of LEV onset with CFD results from a companion research effort shows that the low-order method predicts the spanwise location for the onset of LEV formation correctly and predicts the angle of attack for LEV onset within 1 degree of the CFD result. In both cases, the numerical method over-predicted the angle of attack for LEV onset by 1 degree. This good agreement shows that the overall approach for the numerical method is correct. The cause for the small discrepancy needs to be determined in future efforts.

An Inviscid Numerical Method for Unsteady Flows over Airfoils and Wings to Predict the Onset of Leading Edge Vortex Formation

by
Sachin Aggarwal

A thesis submitted to the Graduate Faculty of
North Carolina State University
in partial fulfillment of the
requirements for the Degree of
Master of Science

Aerospace Engineering

Raleigh, North Carolina

2013

APPROVED BY:

Dr. Andre Mazzoleni	Dr. Jack Edwards

Dr. Ashok Gopalarathnam
Chair of Advisory Committee

DEDICATION

To my Grandparents for believing in me and to my parents for their constant support.

BIOGRAPHY

Sachin Aggarwal was born to Hanuman and Kumkum Aggarwal March 17th, 1988 in Sardarshahr, Rajasthan,India. In 1991, Sachin joined school to get his long journey of education started. He attended his elementary and middle school education in his Hometown. Then he moved to Kota for his high school. He graduated from Aklank Public School in 2005. Sachin started his undergraduate career as Bachelor of Technology in Aerospace Engineering at Amity Institute of Aerospace Engineering Research and Studies, Noida, Uttar Pradesh, India. During summer of 2009 he got the chance of doing a Vocational internship at Hindustan Aeronautics Limited(HAL), Aircraft Divison, Nasik, India. He graduated with B.Tech in Aerospace Engineering after four years of combination of studies and fun in May 2010. After graduation he got an opportunity to work for HAL at Engine divison, Bangalore as a Contract engineer for less than a year time. In August of 2011, he began his pursuit of a Masters of Science in Aerospace Engineering. Sachin joined the NCSU Applied Aerodynamics Research Group under the supervision of Dr. Ashok Gopalarathnam shortly after beginning graduate school. After the completion of his Masters Degree, Sachin will like to join industry as soon as possible

ACKNOWLEDGEMENTS

I would like to thank my advisor Dr. Ashok Gopalarathnam for his guidance and teachings during the past two years at NC State. He played an important role in successful completion of my masters. I also want to thank him for recommending me to MAE department for teaching assistantship which helped me a lot financially from summer of 2012. I am also grateful to Dr. Jack Edwards and Dr. Andre Mazzoleni for consenting to be on my advisory committee.

I want to thank Dr. Jack Edwards and Minao Shen for thier early CFD results that I have used in my thesis.

I am thankful to MAE department at North Carolina State University for funding me throughout my second year of masters. I am also thankful to Mrs. Annie Erwin for helping me with the amount of paperwork that came throughout my graduate school period and for having solution for every problems that I faced during my studies. I also want to extend my thanks to the event team at University Recreation and Creamery at D.H. Hill Library for the opportunity to support myself with the living expenses by making new friends and working as a team.

Special thanks to my parents and my family, for everything.

A big thank you to Kiran for constantly keeping up with my questions about his research and for helping me with a lot of resources that made my research run a lot smoother. I would like to thank Charles Jenckes for sharing his knowledge and experience with me. I also want to thank my research group-mates Shreyas, Aditya, Justin, Ryan, Dhruv, Yoshi and Kristen for their support and fun times.

I would also like to thank my friends and roommates in Raleigh who made the stay enjoyable:

Ray, Sidd, Karan, Khandu, Girish, Swamy and Tejas. Thanks in particular to Sneh and Rushil for amazing trips and fun times we had together and for keeping my morale high through my most stressful days.

TABLE OF CONTENTS

LIST OF TABLES

LIST OF FIGURES

Chapter 1

Introduction

Since ancient times man has been enchanted by the flight of the birds and insects. He has yearned to fly like the birds, and 110 years ago the Wright brothers made it possible by flying the first powered, heavier-than-air aircraft in 1903. Since then we have learned so much more about aerodynamics, which had mesmerized our ancestors. But there are aspects of aerodynamics that elude our understanding and we are trying to decipher it day by day. Around $10,000$ species of birds and nearly a million species of insects use flying as the means of locomotion [3]. Most of them use flapping wings in order to be able to fly. The knowledge of aerodynamic forces in the flapping flight, helicopter rotor dynamics and wind power devices is incomplete partly because of the lack of understanding of the unsteady forces produced by the wings and rotors during the high amplitude flights. The highly complex kinematic movements of the insects and birds wings, the vortical flow structure, their effects on forces and moments, and radial variation of velocity on rotors of helicopter and wind-power devices make it difficult to understand the unsteady regime of aerodynamics.

1.1 Background

Unsteady flow is a major part of low speed aerodynamics. Unsteady flow phenomena occur in a wide range of problems in current aerospace engineering research. These include, but are

not limited to: rotorcraft dynamic stall, delta-wing aerodynamics, wind-power devices, insect flight modeling and micro air vehicle (MAV) design. The recent thrust in research on unsteady aerodynamics has been primarily motivated by interest in aerodynamic modeling of micro air vehicles (MAVs). The small sizes and low flight speeds required of MAVs necessarily result in low Reynolds numbers and lead to high dimensionless rates of motion [4].

Unsteady Aerodynamics has been studied since early 1920's and 1930's. Theodorsen's classical approach gave velocity potential functions to solve the pitching and plunging flat-plate with a flap using two dimensional elementary flows [5]. He assumed a flat wake behind the flat-plate and small amplitude of the motions. Wagner solved the problem of abruptly-starting inclined airfoil at a constant angle of attack which was at rest initially,and came up with the behavior which is now called the "Wagner effect" [6]. He showed that the airfoils start with the half of the steady lift and asymptotically approaches the full value. Garrick further extended the Theodorsen approach and developed the method for determining the thrust force for flat-plate undergoing unsteady motion [7]. Garrick also showed that Theodorsen's and Wagner's theories were equivalent [8]. Von Kármán and Burgers developed a function for the vorticity at the leading edge and calculated the limit as radius of leading edge approaches zero to evaluate the leading edge suction velocity [9]. K*ü*ssner developed a function to show how the lift changes as a function of time as an airfoil experiences a sharp-edged gust [10]. This function was similar to Wagner's and Theodorsen's functions. Von Kármán and Sears generalized the theory of unsteady aerodynamics of an airfoil in non-uniform motions [11]. Loewy investigated the rotary wing with no forward velocity as in hovering scenario and developed a similar solution as Theodorsen with the assumptions of small disturbances [12].

The most important aspect of flapping flight at low Reynolds number flow regimes is the formation and shedding of leading edge vortices (LEV). LEV formation occurs due to the flow separation and shear layer formation at the wing leading edge at high angles of attack. A vortex is developed from this shear layer and travels downstream towards the trailing edge. LEV formation is a precedent to the phenomenon of dynamic stall in rotary-wing aerodynamics. This

LEV enhances the lift for a short-term while it remains attached to the wing. The unsteady motions of the wings in biological flight process provides this short-term prevention of the full development of stall on the wings, hence leads to the success of these large amplitude motions in low Reynolds number flow regimes. The understanding of the causes of this phenomenon has become very necessary in order to successfully replicate its use for agile MAVs.

Weis-Fogh first observed unusually high C_L values from flapping wing insects and attributed the high C_L to the "clap-and-fling" motion executed before the downstroke [13]. He speculated the formation of vortex near the leading edge of flapping wing due to this flinging motion. Maxworthy later confirmed the formation of vortex near the leading edge during the fling process and showed that the LEV stays attached during the downstroke [14]. Ellington & Van den Berg [15] and Ellington et al. [16] revealed the presence of LEV and a highly three-dimensional flow pattern in insect flight using a mechanical flapper which mimicked the motion of a hovering hawkmoth's wings. Dickinson and Birch explained the spanwise flow and the attachment of the LEV on insect wings by using a dynamically scaled insect model [17]. Dickinson et al. further investigated the flow structure of the LEV and force production on the flapping wings at high and low Reynolds numbers [18]. An experimental study and finite-element based analysis of the aerodynamics of insect-based hover-capable flapping wings for MAVs is carried out by Singh and Chopra [19]. These and other research efforts have helped us improve our understanding of the unsteady aerodynamics of insect flight.

The phenomenon of dynamic stall in helicopters prompted many studies of unsteady aerodynamics from the 1970s onwards. McCroskey defined dynamic stall as the unsteady separation and stall phenomena on airfoils that are forced to execute time-dependent motion, oscillatory or otherwise [20]. This phenomenon is characterized by a delay in the onset of flow separation and the shedding of concentrated vorticity from the leading edge of the airfoil. Leading edge vortex formation leading to the dynamic stall is the main reason of high frequency vibrations and unexpected loads on the helicopter blades in forward flight, resulting in potential structure failure in helicopter rotor blades. Leading edge vortices also affects wind power generating

devices as they lead to the dynamic stall of the rotating blades in some operating conditions. Carr investigated the progress in the understanding of dynamic stall and its prediction [21]. In the last 30 years many research efforts using computations and experiments have improved our understanding of leading edge vortex shedding and dynamic stall. Reliable low-order prediction methods, however, are still forthcoming.

To implement the effects of LEV formation in the low-order methods we need to understand the conditions at which the LEV starts forming. In other words, we need to develop a reliable criterion for the prediction of the onset of LEV formation. A computational approach for the rapid and systematic prediction of dynamic stall in unsteady motions was developed by Jones and Platzer [22]. They combined an unsteady two dimensional panel code with a two dimensional boundary layer code. Geissler and Haselmeyer [23] investigated experimentally and numerically the complex flow phenomenon during the onset of dynamic stall. Kriegseis et al. [24] developed a criterion for LEV separation on unsteady aerodynamic profiles using free-surface water tunnel experiments with five airfoils having different leading edge shapes. A number of semi-empirical methods for dynamic stall onset have been developed by Nangia [25] and Leishman & Beddoes [26]. Ramesh et al. [27] developed a criterion for predicting leading edge vortex formation using a new "leading edge suction parameter" (LESP). LESP is a measure of the suction peak attained at the leading edge. This LESP predicts the onset of separation and reattachment of the flow at leading edge and is dependent only on the airfoil shape and Reynolds number, and is independent of the motion kinematics. In this thesis, the LESP concept is extended to use with the lumped vortex element approach.

Moving to LEV formation on three-simensional wings, a rich body of literature is available on experimental and computational studies describing the formation and the prediction of the onset of LEVs. Reliable low-order method models for rapid prediction and design, however, are still not available. Belotserkovskii [28] investigated several methods to study the unsteady aerodynamics of the lifting surfaces using the computer. Methods based on Navier-Stokes and Euler equations solvers in 3D and on potential-flow theory have been developed. Kwak and

Rogers developed an algorithm for the solution of incompressible Navier Stokes equations in three dimensional steady-state and time-dependent flow problems [29]. The Navier-Stokes and Euler equation solver based methods are highly accurate, but are very time consuming and costly because of the small meshes needed for boundary layer resolution, making them inefficient in the earlier stages of the aircraft design. Visbal et al. studied in detail the three-dimensional unsteady leading edge vortex formation induced by large amplitude heaving oscillations of a low-aspect-ratio wing under low Reynolds number conditions and its evolution as it detaches and reattaches. They used a large-scale, free surface water channel for experiments and the parallel high-order FDL3DI Navier-Stokes solver for the computations [30]. Yilmaz and Rockwell studied the flow structure on finite-span wings due to pitch-up motion [2]. Their main objective was to determine the onset and evolution of the three-dimensional leading-edge vortex and to provide complementary interpretations of the vortex structure in terms of streamlines, projections of spanwise and surface-normal vorticity, and surfaces of constant values of the second invariant of the velocity gradient tensor.

Due to their ease of use and low computational costs, potential-flow-theory based methods have been widely adopted for analysis of finite wings for attached flow conditions The most widely used is Vortex Lattice Method (VLM); its historical evolution is described in detail by De Young [31]. The now classical steady VLM was developed by Hedman [32]. Many limitations of this method have been addressed and overcome by several people. VLM was extended to the time-domain unsteady vortex lattice method, generally called UVLM. Many versions of UVLM have been discussed and used for some specific problems. Katz and Levin developed a UVLM to analyze the wake structure and the forces on a delta wing undergoing nonsteady motions [33]. A generalized VLM for calculating unsteady, incompressible, inviscid, three dimensional flows around arbitrary plan-forms have been developed by Mook et al. [34]. Fritz and Long developed an object oriented unsteady VLM based computational method to study the aerodynamics of high reduced frequency flapping flight of small birds and MAVs [35]. The inclusion of effects of the leading edge separation in the calculation of aerodynamic coefficients of lifting surfaces was

first addressed by Mook and Maddox [36]. The applications of unsteady VLM were reviewed and discussed by Murua et al. [37]. Smith et al. investigated the advantages of an unsteady panel method in modeling the aerodynamic forces on rigid flapping wings [38]. In his thesis research effort, Bueso developed a potential flow solver for unsteady aerodynamics of moving aircraft in a MATLAB environment [39]. He investigated two aircraft configurations, classical and with canard. These research efforts have provided us the insight in the capability and feasibility of the potential-flow-theory bases methods.

1.2 Research Objectives

The focus of this research is to develop a numerical method based on discrete vortex lattice model in order to understand the unsteady forces produced by the birds and insects during highly maneuverable flight conditions, such as hovering, non-periodic motions and the forces in helicopter rotor-blade dynamics. This research effort is the first step towards a larger objective, which is to increase the ability of this low-order potential flow method approach to account for the effects of the leading edge vortex shedding and to control these effects for particular flight conditions. The eventual goal is to achieve the results like those presented by Visbal et al. [30] and Rockwell & Yilmaz [2] by using this computationally inexpensive numerical method. The numerical method for two-dimensional flows is based on lumped vortex element approach with some modifications given by Katz and Plotkin in [40], since it is much easier to extend to three dimensional flows than the Fourier series approach used by Ramesh et al. [27].

The two-dimensional numerical method predicts the onset of the leading edge vortex formation during the large amplitude unsteady motions by defining a LESP criterion independent of the body's motion kinematics in both two dimensional and three dimensional aspects of the problem. The validity of the two dimensional part of the numerical method is carried out with the results from the theoretical method developed by Ramesh et al. and the computational and experimental results used in Ref. [41]. Further work on the two dimensional approach is being done at NCSU Applied Aerodynamics Group by the same authors. The three dimensional

extension of the numerical method is based on UVLM formulation. The validity of the three dimensional numerical method is carried out by comparing results from the numerical method with the results for cases of sudden acceleration and heaving oscillations motions given by Katz and Plotkin [40]. A steady state validation is also carried out for the three dimensional extension using simplified VLM given by Weissinger and Athena Vortex Lattice code by Drela [42].

1.3 Layout of Thesis

The unsteady lumped vortex-element approach that forms the core of the two-dimensional low-order numerical method for inviscid analysis of large-amplitude, high-frequency motions, is described in Chapter 2. To evaluate the inviscid criterion for determining the start of LEV formation, a new approach to determine a parameter similar to LESP is also introduced in Chapter 2. Chapter 3 validates the hypothesis presented towards the development of the numerical method by comparing results from the computations, experiments and the theoretical method. The approach towards the three-dimensional extension of the numerical method is discussed in Chapter 4. The results from the three-dimensional extension of numerical method are presented and validated in Chapter 5. Chapter 6 concludes the thesis with some observations and discussions on the feasibility and future possibilities on the evolution of the numerical method.

Chapter 2

Two-Dimensional Numerical Method for Onset of LEV Formation

In this research effort a time-stepping approach based on lumped-vortex element method similar to the one given by Katz and Plotkin [40] is used with modifications to predict the onset of LEVs using a parameter similar to the LESP [41]. The LESP is a parameter developed to determine the "start" and "stop" criteria for LEV shedding [27]. In the research performed by Ramesh et al. [27], an unsteady thin airfoil theory was used as the foundation for studying LEV-dominated flows. In that theory, the bound vorticity distribution on the airfoil was modeled using a Fourier series. It was shown [41] that the LESP was simply the A_0 term of the Fourier series, such that when the LESP crosses a critical value, LEV shedding is "on". The drawback with the Fourier-series based airfoil theory is that there does not seem to be any natural way to extend the approach to three-dimensional analysis of finite wings. This drawback has provided the motivation for the current work. By developing an LESP-like criterion for a 2D lumped vortex method, the goal is to be able to extend the LESP criterion to 3D wing analysis using vortex lattice methods. This chapter describes the 2D lumped-vortex element method and the modification to predict the onset of LEV formation.

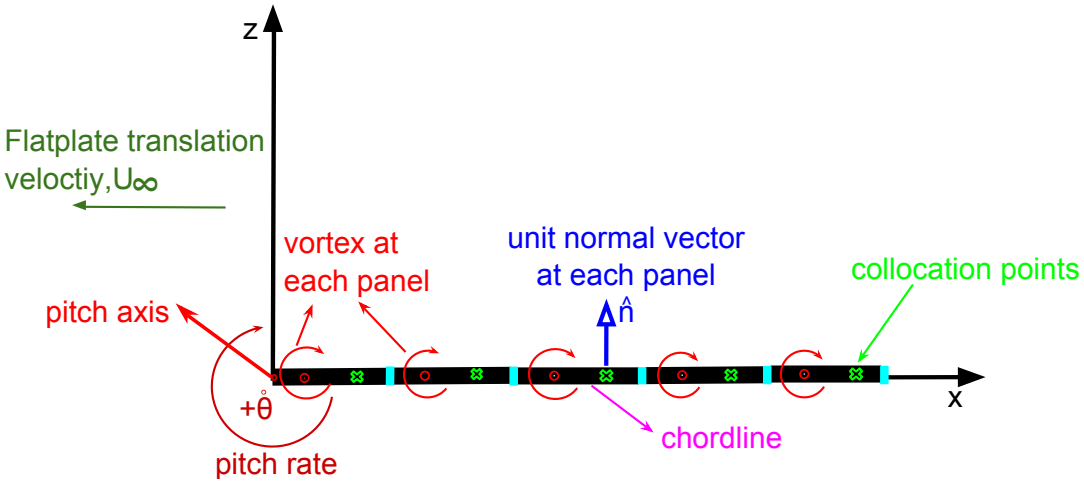

Figure 2.1: Discrete vortex model for the unsteady thin uncambered airfoil/flat plate

2.1 Methodology

2.1.1 Geometry Definition

Geometry generation and discretization is implemented through the lumped vortex element method where the airfoil is represented by means of N discrete vortices on the camberline. The camber-line is defined using a surface function called $\eta(x)$. The surface function is evaluated using the average of the aligned coordinate points on the upper and lower surface of the airfoil. For the aligned coordinate points, first the airfoil profile is made by interpolation of input coordinate points from XFOIL into a smooth fit, and then the airfoil's upper and lower surface is divided equally along the chordline. The camberline is divided into N number of sub-panels that are equal in length. For a flat-plate or uncambered airfoil the chordline is the camberline, so sub-panels are created using chordline. The bound vortices are placed at quarter chord of the sub-panels and collocation points at three quarter chord point of each sub-panel. At these collocation points the zero normal flow boundary condition is fulfilled. The unit normal vector at each sub-panel is also defined, as shown in the uncambered airfoil geometry plot in figure 2.1 and cambered airfoil geometry plot in figure 2.2.

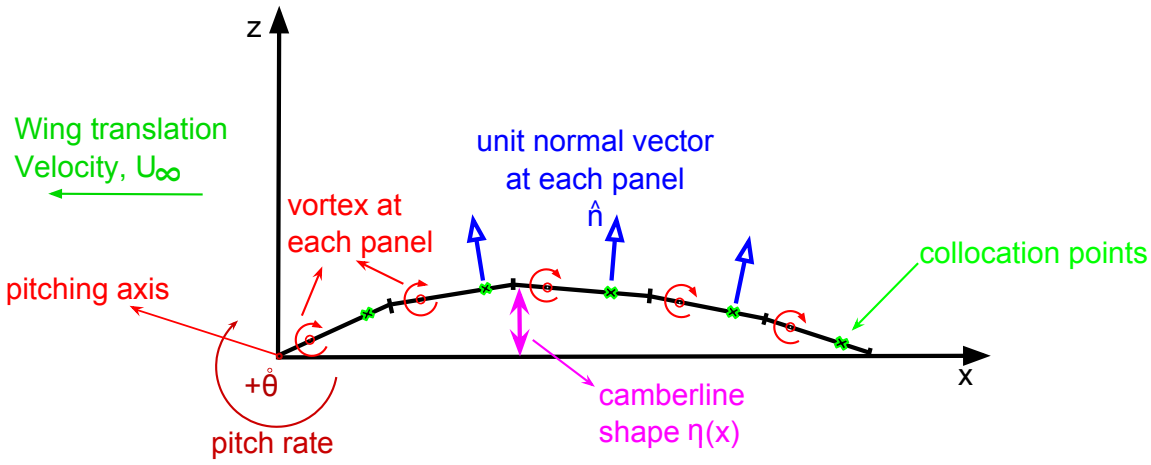

Figure 2.2: Discrete vortex model for the unsteady thin cambered airfoil

2.1.2 Influence Coefficients and Boundary Conditions

Two coordinate system are selected: (1) the inertial frame of reference and (2) the body-fixed reference frame attached to the airfoil. The position of body-fixed reference frame on the airfoil is dependent on the pivot location about which it is rotating. At time t = 0, the body-fixed reference frame coincides with the inertial reference frame as the body is stationary. At time $t > 0$, the body- fixed reference frame moves to the left of the page as the airfoil starts moving with velocity of U_∞. A trailing edge vortex is shed at every time step to satisfy the Kelvin's condition, so that for any positive change in airfoil circulation an equal and opposite strength trailing edge vortex is shed. Therefore, if the body's circulation is varying continuously, a series of wake vortices is shed. Figure 2.3 shows the model with wake vortices after five time steps.

The zero normal flow boundary condition in the time dependent case is given by

$$\left(\nabla\vec{\phi}_B + \nabla\vec{\phi}_w - \vec{V}_0 - \vec{v}_{rel} - \vec{\Omega}\times\vec{r}\right)\cdot\hat{n} = 0 \tag{2.1}$$

The normal component of the total velocity at each collocation point is calculated by adding the self induced velocity due to the vortex at each panel, the kinematic velocity, and the velocity

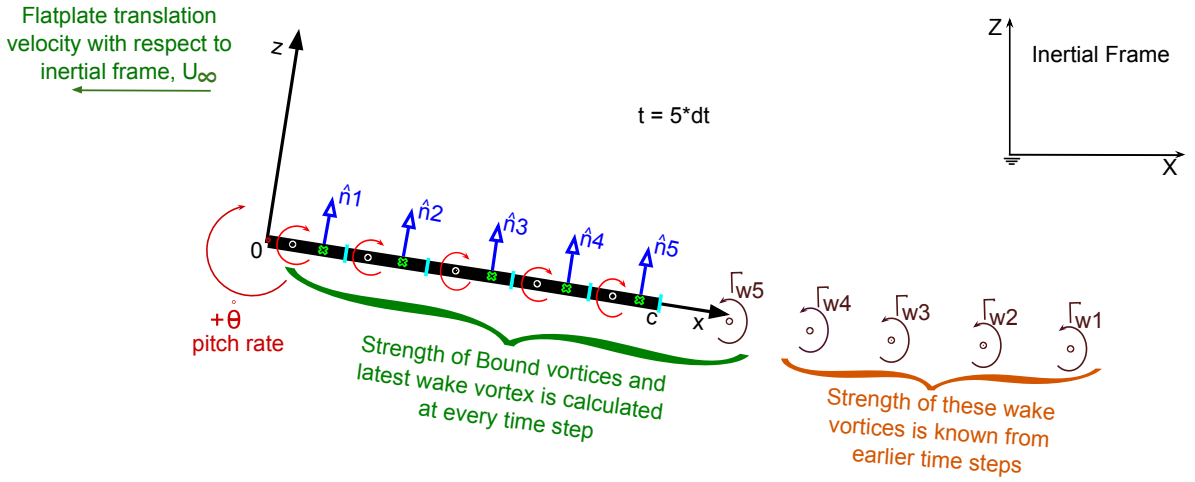

Figure 2.3: Discrete vortex model with wake vortces after five time steps for the flat plate

induced due to the shed vortex (wake vortex). The self induced component, $\nabla\vec{\phi}_B \cdot \hat{n}$, from equation 2.1 at each collocation point is calculated by the velocity induced by the airfoil bound vortex points. By assuming unit strength vortex at each panel we calculate the influence of each vortex on each collocation point and we call it as the influence coefficient matrix. The following equation gives the (i, j) element of the influence coefficient matrix:

$$IC_{ij} = (u, w)_{ij} \cdot \hat{n}_i \tag{2.2}$$

where u and w are the velocity components induced at collocation point i by the airfoil's unit strength vortex at j element and $\hat{n}_i$ is the unit normal vector of the panel. They are calculated using the equation of downwash at a point due to a unit vortex ($\Gamma_j = 1$) given by,

$$u_{ij} = \frac{\Gamma_j}{2\pi r}(z_i - z_j) \tag{2.3}$$

$$w_{ij} = \frac{\Gamma_j}{2\pi r}(x_i - x_j) \tag{2.4}$$

$$r = (x_i - x_j)^2 + (z_i - z_j)^2 \tag{2.5}$$

The normal and tangential unit vectors at each sub-panel are evaluated using the equations:

$$\hat{n}_i = \frac{\left(-\frac{\partial \eta}{\partial x}, 1\right)}{\sqrt{\left(\frac{\partial \eta}{\partial x}\right)^2 + 1}} = (\sin\alpha_i, \cos\alpha_i) \tag{2.6}$$

$$\hat{\tau}_i = (\cos\alpha_i, -\sin\alpha_i) \tag{2.7}$$

and for uncambered airfoil the normal vector becomes $\hat{n}_i = [0, 1]$.

The kinematic velocity component is calculated using the transformation of coordinate systems. The velocity components observed in body-fixed reference frame due to the kinematic motion are given by,

$$\begin{pmatrix} U_t \\ W_t \end{pmatrix} = \begin{pmatrix} \cos\theta(t) & -\sin\theta(t) \\ \sin\theta(t) & \cos\theta(t) \end{pmatrix} \begin{pmatrix} -\dot{X}_0 \\ -\dot{Z}_0 \end{pmatrix} \tag{2.8}$$

Here $-\dot{X}_0$ and $-\dot{Z}_0$ are the velocity components in the inertial frame.

The final time-dependent kinematic velocity components including the rotation in body-fixed reference frame and the plunge rate of the airfoil, $\dot{h}$ is given as

$$\begin{pmatrix} U_t \\ W_t \end{pmatrix} = \begin{pmatrix} \cos\theta(t) & -\sin\theta(t) \\ \sin\theta(t) & \cos\theta(t) \end{pmatrix} \begin{pmatrix} -\dot{X}_0 \\ -\dot{Z}_0 \end{pmatrix} + \begin{pmatrix} \dot{h}\sin\alpha - \dot{\theta}\eta \\ \dot{\theta}x - \dot{h}\cos\alpha - \frac{\partial \eta}{\partial t} \end{pmatrix} \tag{2.9}$$

The flight path of the origin in the body-fixed reference frame with respect to inertial reference frame is given by following equation:

$$\begin{pmatrix} X \\ Z \end{pmatrix} = \begin{pmatrix} \cos\theta(t) & \sin\theta(t) \\ -\sin\theta(t) & \cos\theta(t) \end{pmatrix} \begin{pmatrix} x \\ z \end{pmatrix} + \begin{pmatrix} X_0 \\ Z_0 \end{pmatrix} \tag{2.10}$$

And the wake induced velocity component, $\nabla\phi_W \cdot n$, from equation 2.1 is calculated at each time step by substituting the bound vortex points with the wake vortex points in equations 2.3 - - 2.5. These wake vortex points are calculated for each time step by placing the latest wake vortex at 0.3 times the distance covered by the trailing edge in that time step. The strength of these wake vortices is calculated using the Kelvin's condition.

2.1.3 Kelvin's Condition

Kelvin's condition states that "In an inviscid flow with conservative body forces, the circulation around a closed curve (which encloses the same fluid elements) moving with the fluid remains constant with time". The strength of each wake vortex is equal to the vorticity shed during that particular time step and is calculated at each time step by satisfying the Kelvin's condition given by,

$$\frac{D\Gamma}{Dt} = 0 \tag{2.11}$$

$$\frac{d\Gamma(t)}{dt} + \frac{d\Gamma_W}{dt} = 0 \tag{2.12}$$

Though we know the wake velocities from previous steps, the current step's wake velocities are unknown as the strength of the latest wake vortex and the bound vortices are unknown. Thus we apply a modified form of Kelvin's condition,

$$\Gamma(t) - \Gamma(t - \Delta t) + \Gamma_{W_t} = 0 \tag{2.13}$$

$$\Gamma(t) = \sum_{j=1}^{N} \Gamma_j \tag{2.14}$$

The final form of zero normal flow boundary condition at i^{th} collocation point can be formulated as:

$$\sum_{j=1}^{N} (IC_{ij} \cdot \Gamma_j) + IC_{iW} \cdot \Gamma_{W_t} + [U(t) + u_W, W(t) + w_W]_i \cdot n_i = 0 \tag{2.15}$$

Now putting together equations for all collocation points with Kelvin's condition equation we get a final equation in matrix form:

$$\begin{pmatrix} IC_{11} & IC_{12} & \dots & IC_{1N} & IC_{1W} \\ IC_{21} & IC_{22} & \dots & IC_{2N} & IC_{2W} \\ \vdots & \vdots & \ddots & \vdots & \vdots \\ IC_{N1} & IC_{N2} & \dots & IC_{NN} & IC_{NW} \\ 1 & 1 & \dots & 1 & 1 \end{pmatrix} \begin{pmatrix} \Gamma_1 \\ \Gamma_2 \\ \vdots \\ \Gamma_N \\ \Gamma_{W_i} \end{pmatrix} = \begin{pmatrix} RHS_1 \\ RHS_2 \\ \vdots \\ RHS_N \\ \Gamma(t - \Delta t) \end{pmatrix} \tag{2.16}$$

where the RHS vectors are evaluated from equation 2.15, given as:

$$RHS_i = -\left[U(t) + u_W, W(t) + w_W\right]_i \cdot \hat{n}_i \tag{2.17}$$

From the above equation 2.16, we can calculate the only unknowns that are the circulation values at each panel and that of the wake vortex shed at the latest time step.

2.1.4 Aerodynamic Calculations

The resulting pressure and loads are computed using the Bernoulli equation near the panel surface,

$$\frac{p_{ref} - p}{\rho} = \frac{Q^2}{2} - \frac{\nu_{ref}^2}{z} + \frac{\partial \phi}{\partial t} \tag{2.18}$$

$$\Delta p = p_l - p_u = \rho \left[\left(\frac{Q_t^2}{2} \right)_u - \left(\frac{Q_t^2}{2} \right)_l + \left(\frac{\partial \phi}{\partial t} \right)_u - \left(\frac{\partial \phi}{\partial t} \right)_l \right] \tag{2.19}$$

The final pressure difference between the upper and lower surfaces becomes,

$$\Delta p_j = \rho [U(t) + u_W, W(t) + w_W]_j \cdot \hat{\tau}_j \frac{\Gamma_j}{\Delta l_j} + \frac{\partial}{\partial t} \sum_{k=1}^{j} \Gamma_k \tag{2.20}$$

As $\hat{\tau}_j = (1, 0)$ for a flat plate ,the pressure difference becomes

$$\Delta p_j = \rho \left[U_\infty \sin(\alpha(t)) \frac{\Gamma_j}{\Delta l_j} + \frac{\partial}{\partial t} \sum_{k=1}^{j} \Gamma_k \right] \tag{2.21}$$

Here the first term $(U_\infty \sin(\alpha(t)) \frac{\Gamma_j}{\Delta l_j})$ is an instantaneous circulatory term and second term $(\frac{\partial}{\partial t} \sum_{k=1}^{j} \Gamma_k)$ is the measure of time-dependency also known as apparent mass effect. The total dimensionless normal force is obtained by integrating the pressure difference equation 2.21 along the camberline:

$$N(t) = \sum_{j=1}^{N} \Delta p_j \, (t) \, \Delta l_j \tag{2.22}$$

$$C_N(t) = \frac{N(t)}{(0.5 \rho U^2 c)} \tag{2.23}$$

Another force that is generated during these motions that contributes to the overall aerodynamic forces is the leading edge suction force. Leading edge suction occurs due to the movement of the airfoil's stagnation point away from the airfoil's leading edge at an angle of attack. This movement compels the flow to travel around airfoil's leading edge to go over other surface. The following section discusses the calculation of the leading-edge suction with the 2D lumped vortex method.

2.1.5 Leading edge suction

In the large angle thin airfoil theory developed by Ramesh et al. [27], the chordwise distribution of bound vorticity is described using a Fourier series as follows, with the Fourier terms being time varying.

$$\gamma \, (\theta, t) = 2U(t)[A_0(t) \frac{1 + \cos \theta}{\sin \theta} + \sum_{n=1}^{\infty} A_n(t) \sin(n\theta)] \tag{2.24}$$

where θ is the angular coordinate given as,

$$\theta = \cos^{-1}(1 - \frac{2x}{c}) \tag{2.25}$$

Of particular interest is the A_0 term in the series. First, as shown in Ref. [41], the leading-edge suction force coefficient is directly proportional to the square of A_0. This force starts to make a noticeable contribution to the total force at large angles of attack. Second, as shown in [27], it is possible to define a parameter called the leading edge suction parameter, or LESP, that characterizes the instantaneous suction at the leading edge. For any airfoil and Reynolds number combination, it can be shown that there is a critical value of the LESP that determines whether the flow at the leading-edge is attached or detached due to LEV shedding. In other words, the LESP can be used to determine the "start" and "stop" conditions for LEV shedding. As shown in [27], the LESP is directly proportional to the A_0 term. Thus the A_0 Fourier term is especially useful in theoretical prediction of LEV-dominated flows.

An important goal of the current effort is to develop a way to determine a parameter similar to the LESP, but from the discrete vortex numerical method. It is clear that the vortex strength of the leading-edge panel can be used as such a parameter. However, as shown in Fig. 2.4, if the LESP is constructed by nondimensionalizing this vortex strength without any modifications, it is dependent on the number of chordwise panels used in the discretization.

We came up with an approach to calculate this parameter using a modification of this bound-vortex strength of the leading-edge panel at each time step. This approach makes this parameter independent of the number of panels used for the discretization in the chordwise direction. This approach attempts to find a scaling relation that matches up the value of Γ_1 (the vortex strength of the leading-edge panel) in the numerical method with the A_0 term in the theory. For this purpose, it is assumed that all the other terms in the Fourier series are negligibly small over the leading-edge panel. In theory, these terms are exactly zero only at the leading edge ($x = 0$). We then assume that the bound vortex strength of the first panel, Γ_1, is

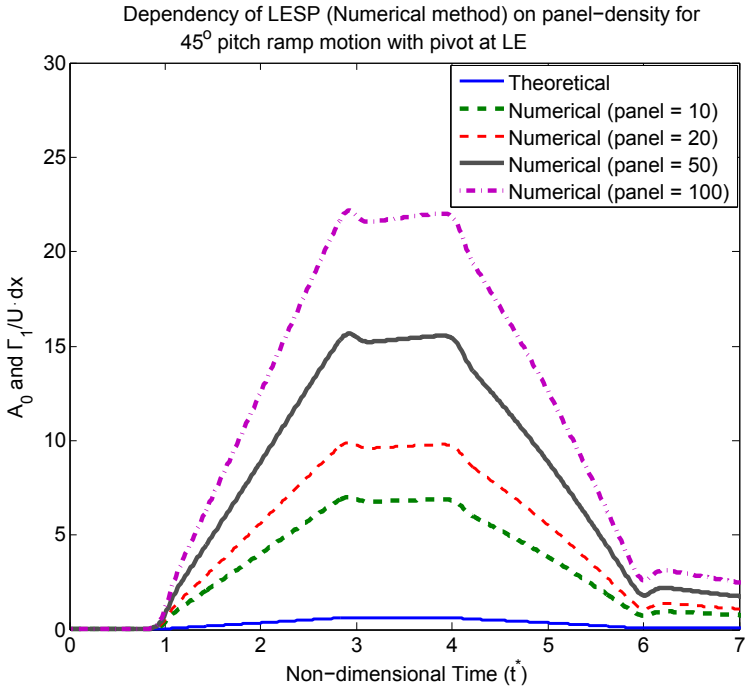

Figure 2.4: Comparison of LESP from the numerical method determined using Γ_1, the vortex strength of the leading-edge panel, with the LESP from the theoretical method determined using the value of the A_0 term

equal to the vorticity distribution over the chordwise length of the first panel (Δl) due to the A_0 term. This results in:

$$\Gamma_1(t) = \int_0^{\Delta l} \gamma\,(\theta, t)\,dx \tag{2.26}$$

where $dx = (c/2)\sin\theta d\theta$ and A_1 to A_N are zero for first panel.

After putting these variables in equation 2.26 we get,

$$\Gamma_1(t) = \int_0^{\Delta\theta} 2U(t)[A_0(t)\frac{1+\cos\theta}{\sin\theta}]\frac{c}{2}\sin\theta d\theta \tag{2.27}$$

$$\Gamma_1(t) = U(t)A_0 c\int_0^{\Delta\theta}(1+\cos\theta)d\theta \tag{2.28}$$

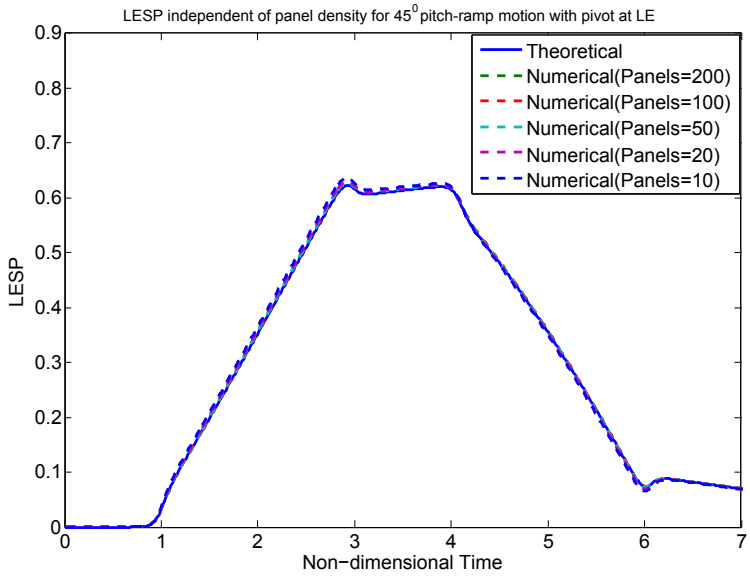

Figure 2.5: LESP comparison independent of panel density for 45^o pitch-ramp motion

where,

$$\Delta\theta = \cos^{-1}(1 - \frac{2\Delta l}{c}) \tag{2.29}$$

Finally after integrating and rearranging the equation, we get,

$$A_0(t) = \frac{1.13 \cdot (\Gamma_1(t))}{U(t)c[\cos^{-1}(1 - \frac{2\Delta l}{c}) + \sin(\cos^{-1}(1 - \frac{2\Delta l}{c}))]} \tag{2.30}$$

Here the "1.13" is an empirically-determined scaling factor that was required to achieve equivalence between the LESP from the numerical and theoretical methods. As seen from Fig. 2.5, the results for this LESP from the numerical method are independent of the discretization and also match excellently with the LESP from the theoretical method. From Ref. [41] the dimensionless suction force is given by,

$$C_S(t) = 2\pi A_0^2(t) \tag{2.31}$$

By using equations 2.23 and 2.31 we can now calculate the coefficient of lift and drag, given by equations:

$$C_L(t) = C_N(t)\cos\alpha\,(t) + C_S\,(t)\sin\alpha\,(t) \tag{2.32}$$

$$C_D(t) = C_N(t)\sin\alpha\,(t) - C_S\,(t)\cos\alpha\,(t) \tag{2.33}$$

where α is the instantaneous angle of attack.

Chapter 3

Two Dimensional Results and Validations

3.1 Results for Uncambered Airfoil

The two-dimensional numerical method is tested for several large-amplitude unsteady motions. These unsteady motions include pitch ramp-hold motions with different pivot locations. The pitch ramp motions were developed by the AIAA FDTC Low Reynolds Number Discussion Group. Eldredge's canonical formulation is used to create the smooth ramp for these motions [43]. By changing the pivot locations from leading edge to trailing edge, motion variations are being studied. Motions with high amplitudes of 25° and 45° are tested with leading edge, half chord and trailing edge as the different pivot locations. The motions are shown in figure 5.3.

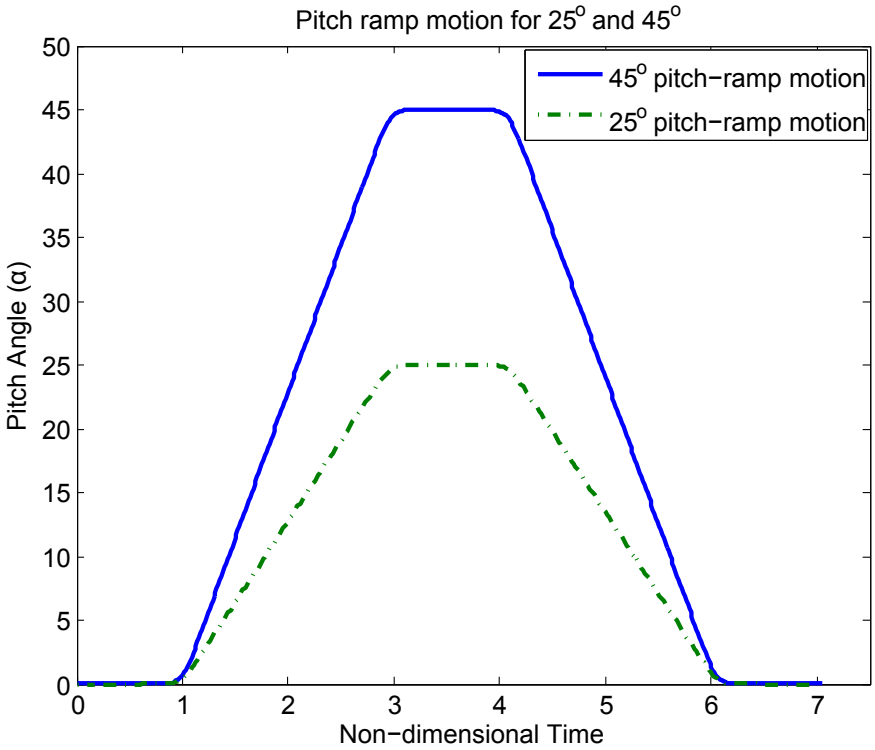

Figure 3.1: Pitch ramp-hold motion for 25^o and 45^o

3.2 Validation of the Numerical Method for Pitch Ramp-Hold Motions

The theoretical method is developed by Kiran Ramesh in his PhD research effort [41]. In this method an inviscid unsteady theory applicable to non-periodic motions is developed that accounts for large amplitude and non-planar wakes. This method uses time-dependent Fourier series to model the chordwise vorticity distribution. To satisfy the Kelvin's condition a Newton-Raphson iteration is carried out at each time-step which gives the strength of the latest shed vortex as per the method discussed in Katz and Plotkin [40].

An incompressible Navier-Stokes solver developed at NCSU was used to perform the computational fluid dynamics calculations employed in this paper [41] for the comparisons. A finite-

volume discretization of the governing equations is used, with an incompressible-limit form of Edwards' all-speed low-diffusion flux splitting scheme (LDFSS) [44, 45] used to formulate the inviscid fluxes at each cell interface. This solver uses an immersed boundary (IB) method [46] to impose the motion of the object - a rounded flat-plate with a chord length of 3 and a thickness to chord ratio of 0.0417. This method in detail is discussed in Ramesh et al. [41].

The experimental results are generated at U.S. Air Force Research Laboratory's Horizontal Free-surface Water Tunnel using a three degree of freedom electric rig which enables independent control of pitch or rotation, plunge or heave and surge or stream-wise-aligned translation. More detail on the rig operation is given in Ol et al. [47] and Granlund et al. [48]. Flow visualization is done using dye injection with a 70/30 percent (by volume) mixture of blue food coloring and ethanol, to match the density of ambient water. Force data are recorded from an ATI Nano-25 IP68 6-component integral load-cell, oriented with its cylindrical axis normal to the pitch-plunge-surge plane. The details about this experimentation is given in Ramesh et al. [41].

The lift coefficients over time from the numerical method of the current work are compared with theoretical, computational and experimental results from Ramesh et al. [41] for three pivot locations. They are plotted and discussed using four critical points in the flow [41]. These critical points are dependent on the pivot locations as well as amplitude of the motions. They are:

- A - onset of flow separation at the leading edge
- B - detachment of the leading edge vortex and the onset of reversed flow on airfoil
- C - hold start
- D - hold end

3.2.1 45^o Amplitude Pitch-ramp-hold Motion

Leading Edge Pivot:-

Figure 3.2 shows the comparisons of the lift coefficient over time for all the four methods with pivot at leading edge. The results from the numerical method are in congruence with the the-

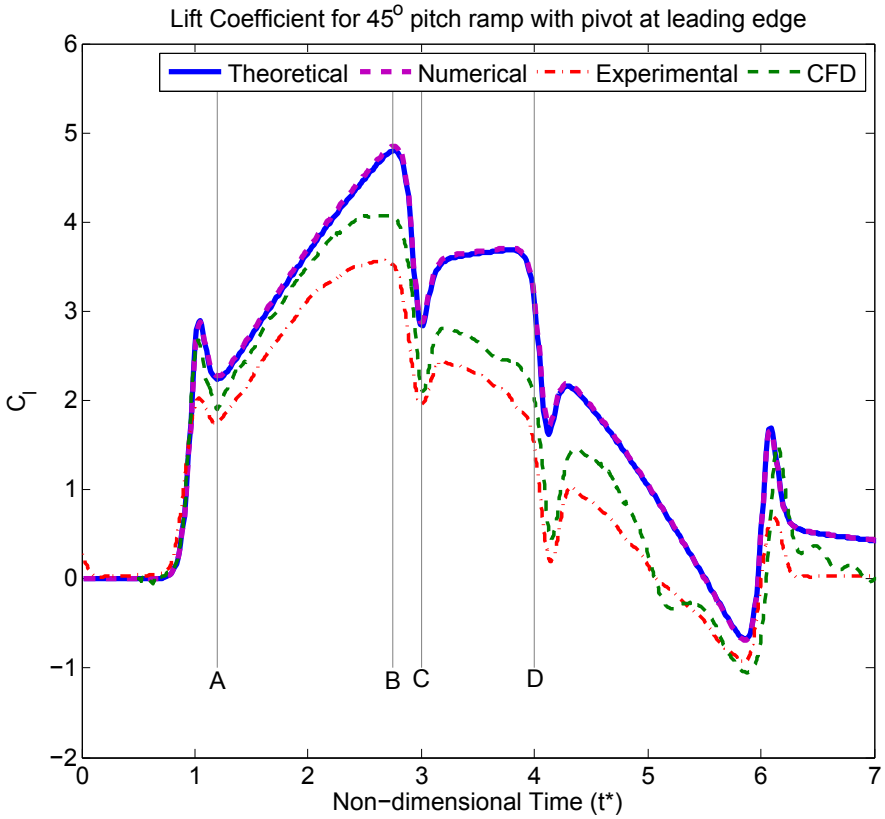

Figure 3.2: Lift coefficient for leading edge pivot

oretical method for full time cycle and match well with computation and experiment on the upstroke even at the large angles of attack. This shows that the numerical method effectively implements the effects of large amplitudes and non-planar wakes. The numerical and theoretical methods over-predict the lift coefficient in the hold and down-stroke because the hold and the down-stroke are dominated by viscous effects. The computational results are matched even better with the experiments than the numerical and theoretical methods. The critical points for this case is marked in figure 3.2. In this case the onset of leading edge separation occurs very early in the upstroke and detachment occurs at the end of the upstroke causing reverse flow early and finally resulting in decrease of lift in the hold and down-stroke stage of the motion. The numerical method is not able to predict this reduction because of large-scale separated

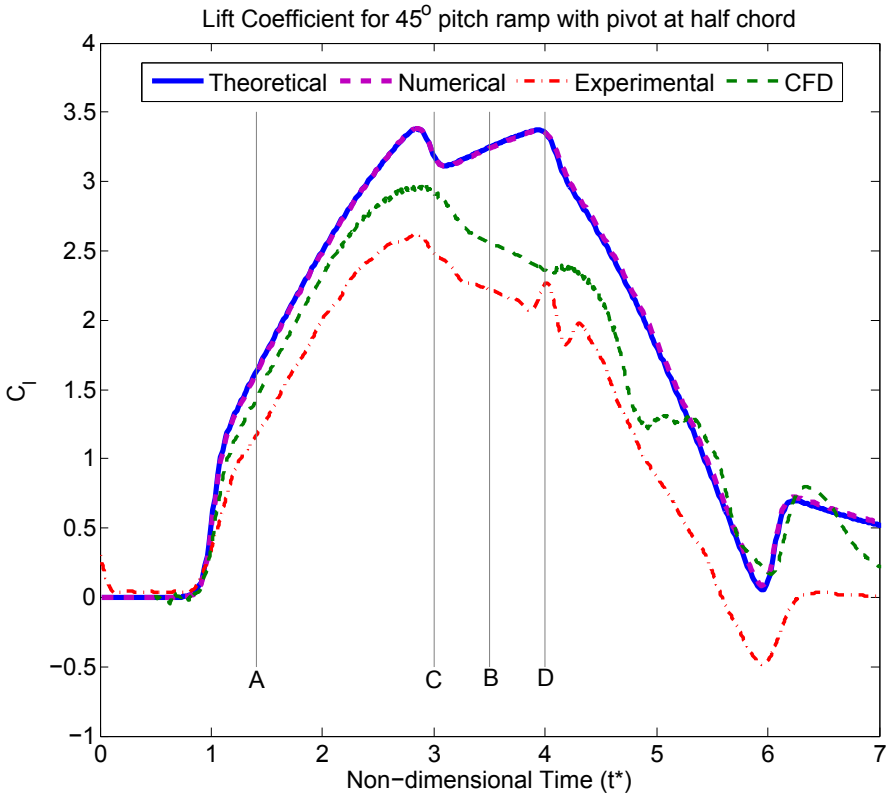

Figure 3.3: Lift coefficient for half chord pivot

flow over the airfoil/flat-plate.

Half Chord Pivot:-

A comparison of the lift coefficients between the four methods, for the 45^o pitch ramp case pitched about half chord is given in figure 3.3. The figure clearly shows that again the results from numerical method and theoretical method are in congruence. The match between results from numerical/theoretical calculations with those from computations and experiments is not as good as for the leading-edge pivot case. There is also an over prediction of lift coefficient in computations compared to experiments in the down-stroke. We can interpret from this, the LEV phenomenon here is similar to the leading edge pivot case except that the two critical

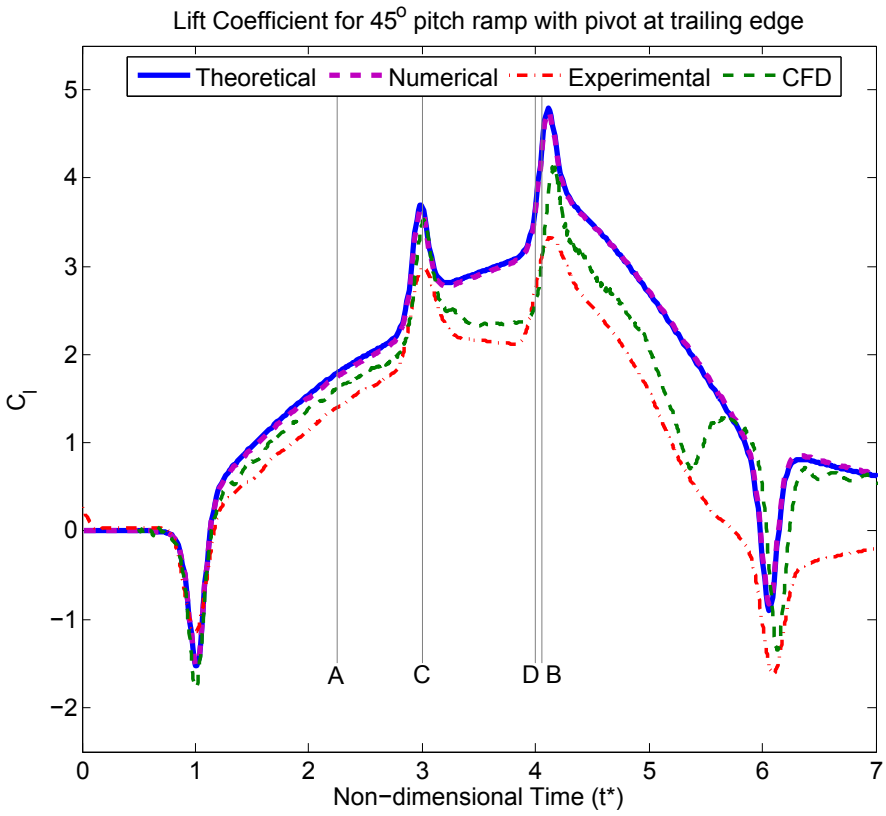

Figure 3.4: Lift coefficient for trailing edge pivot

points i.e. A and B are delayed as a result of pivot movement from leading edge to half chord.

Trailing Edge Pivot:-

Similar to leading edge and half chord pivoted cases a comparison of the lift coefficients between numerical method, theoretical method, computations and experiments is shown in figure 3.4. This figure shows the same trends of comparisons of the results as from the other two cases for 45^o pitch-ramp motions.

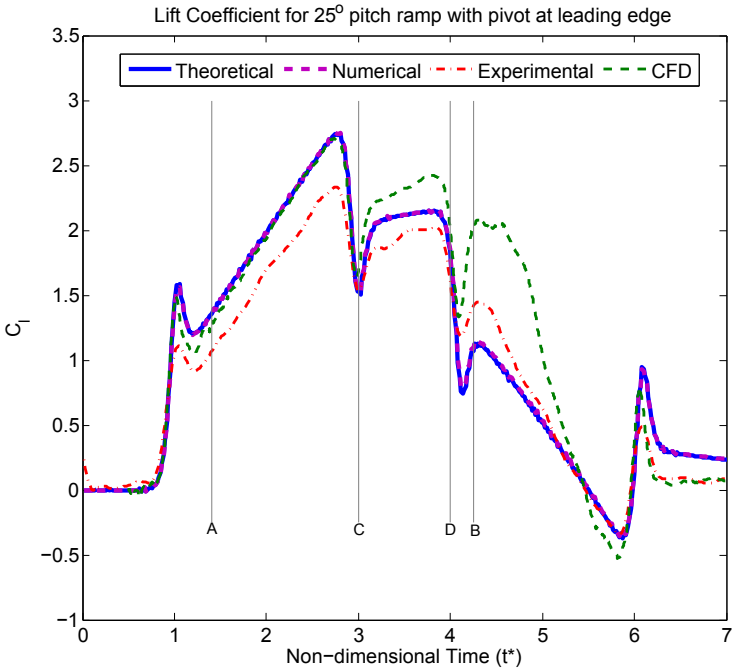

Figure 3.5: Lift coefficient for leading edge pivot

3.2.2 25^o Amplitude Pitch-ramp-hold Motion

A similar approach of discussing results as in 45^o pitch ramp motion cases is used for the interpretation of the results for 25^o pitch-ramp motion cases. In the 25^o cases the onset of leading edge separation occurs early in the upstroke but relatively later than 45^o cases initiating the formation of the LEV. The flow then reattaches on the upper surface of the airfoil keeping the LEV attached for the motion ahead until it approaches towards the trailing edge in the down-stroke, where it separates. The separated LEV moves over the chord during the rest of the down-stroke causing the flow reversal on the surface of the airfoil and resulting in the lift coefficient increase.

Leading Edge Pivot:-

The comparisons of the lift coefficients between numerical method, theoretical method, computations and experiments is co-plotted in figure 3.5 and critical points are also marked. The

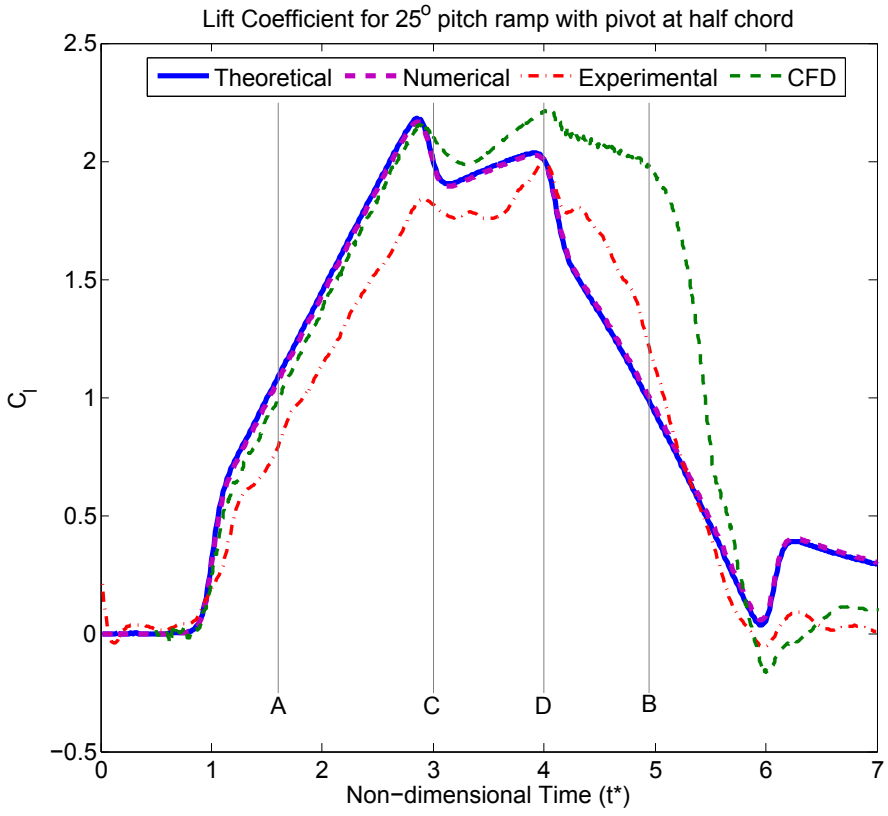

Figure 3.6: Lift coefficient for half chord pivot

results from numerical method as before match excellently with those from the theoretical method. These also match reasonably well with the computations and experiments except in LEV-dominant portions of the motion.

Half Chord Pivot:-

A comparison between the lift coefficients from the four methods, for the 25^o pitch ramp case pitched about half chord is given in figure 3.6. We can interpret from the plot that the LEV phenomenon here is similar to the leading edge pivot case. The trends in the results are similar to those seen in the leading-edge pivot case.

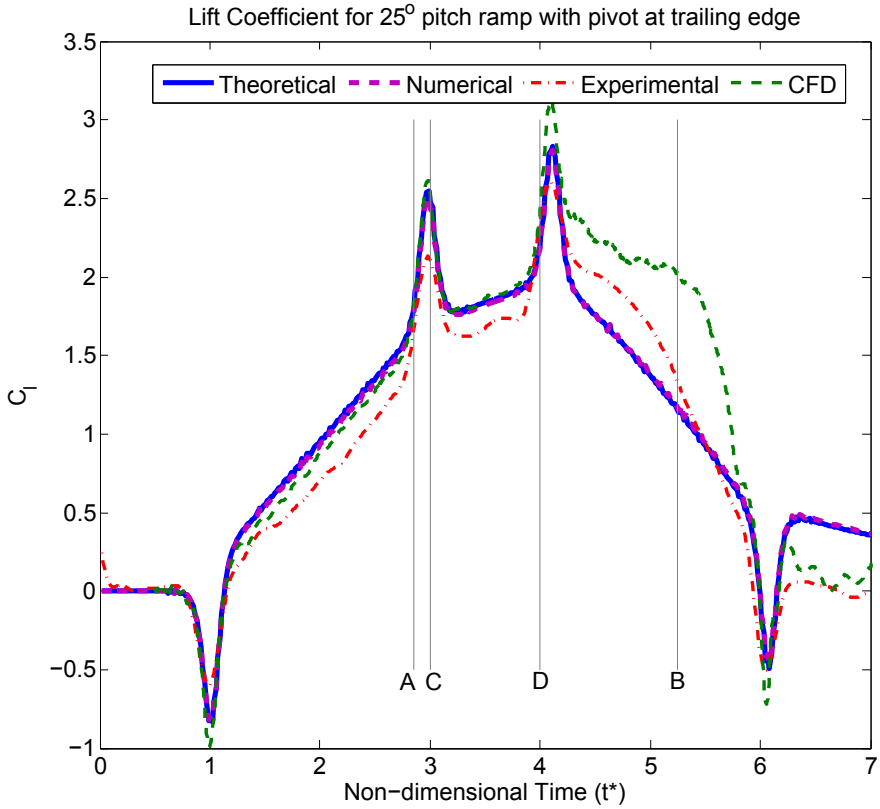

Figure 3.7: Lift coefficient for trailing edge pivot

Trailing Edge Pivot:-

Figure 3.7 shows the comparisons similar to above cases for uncambered airfoil/flat-plate pivoted at trailing edge.

3.3 Discussion

We observed from the plots above that there is small deviations in the lift coefficients of numerical method with computations and experiments in some places. This deviation is because the numerical method does not take account the LEV phenomenon and the viscosity effects. Lift coefficients from the computations and experiments in the hold region have a decreasing trend

for the 45^o cases and increasing trend for 25^o cases while the numerical method and theoretical method deduce an increasing trend in the hold region because the wakes effects decreases as they move downstream. In experiments and computations for 45^o cases hold region sees a detached LEV which results in decrease of the lift while for 25^o cases hold region has reattachment of LEV so the lift increases as compared to the numerical and theoretical method results.

Chapter 4

Three Dimensional Extension of the Numerical Method

The numerical method is extended to solve three-dimensional problems. In real life scenarios there would be a finite span for the wing or rotor-blade which is going through unsteady motion. The classical unsteady aerodynamics theories are not able to explain the extra lift production in the unsteady motions because they do not take into account the leading edge wake shedding effects. By using the three dimensional numerical method we will be able to predict the onset of LEVs on the finite span lifting surfaces. These LEVs are the main contributors to the extra lift generated in the high dimensionless rates of time-dependent motions. These LEVs make it possible for birds to carryout some highly maneuverable motions like hovering in low flow velocities and also are responsible for higher loads on the helicopter rotors and wind-power generating blades leading to structure failure. This method will be a stepping stone towards the explanation of the extra lift that governs the unsteady aerodynamics in flapping flight, helicopter rotor dynamics and wind-power devices, and its effects on the stability and control of the wing and blade.

4.1 Approach

The major differences between the 3D and 2D methods is that in 2D, we were assuming an infinite length vortex placed on the quarter chord of the panel while in 3D we will have a finite length uniform strength vortex filament. The wing will be divided in both span-wise and chord-wise directions to form equally sized panels. A uniform strength bound vortex filament is placed on the quarter chord of the panel and each side represent the trailing vortex filament. This creates a vortex ring on each panel whose four sides are assumed to have the same vortex strength. The induced effect of this ring on any point is calculated using Biot Savart's law.

4.1.1 Biot-Savart's Law

Biot-Savart's Law states that the velocity induced at a point $\vec{R}(R_x,R_y,R_z)$ due to a line vortex segment of uniform strength starting from $\vec{S}(S_x,S_y,S_z)$ and ending at $\vec{E}(E_x,E_y,E_z)$ where direction of vorticity is from $\vec{S}$ to $\vec{E}$ is given by:

$$\vec{V} = \frac{\Gamma}{4\pi} q_1 \left(\vec{R}, \vec{S}, \vec{E}\right) \tag{4.1}$$

where q_1 is a function of $\vec{R}$, $\vec{S}$ and $\vec{E}$ given as

$$q_1 \left(\vec{R}, \vec{S}, \vec{E}\right) = \frac{\left(\vec{a} \times \vec{b}\right)}{\left(\vec{a} \times \vec{b}\right) \cdot \left(\vec{a} \times \vec{b}\right)} \left(\mid \vec{a} \mid + \mid \vec{b} \mid\right) \left(1 - \frac{\vec{a} \cdot \vec{b}}{\mid \vec{a} \mid\mid \vec{b} \mid}\right) \tag{4.2}$$

where $\vec{a} = (\vec{S} - \vec{R})$ and $\vec{b} = (\vec{E} - \vec{R})$

4.2 Methodology for 3 D method

The current 3-D numerical method follows the flow chart shown in figure 4.1, which shows the major steps carried out in the program. This methodology is based on the unsteady lifting-

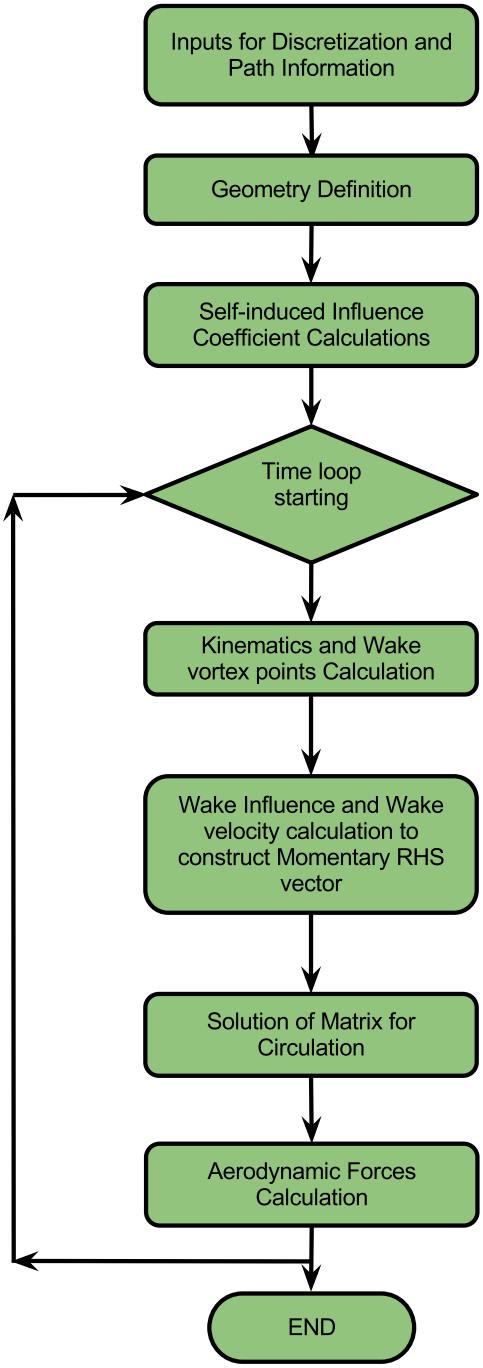

Figure 4.1: Flow chart showing three dimensional method processes for flat plate wing

surface solution by vortex ring elements and time stepping approach from Low Speed Aerodynamics by Katz and Plotkin [40].

4.2.1 Geometry

The geometry of the wing is defined using the coordinate points of the four corners of the wing from the input file. This geometry is discretized then equally in span-wise as well as chord-wise direction. The number of divisions (L in chord-wise and M in span-wise direction) are also specified in the input file. A vortex ring is created at each panel using two bound vortices and two trailing vortices. The first bound vortex is placed on the quarter chord of the panel and the second on the quarter chord of panel downstream. The trailing vortices are on the sides. For the trailing edge panels the second bound vortex is placed at $0.2 - 0.3$ times the distance moved by the wing in first time step; that is, $(0.3Q\Delta t)$. The collocation points are also defined for each panel at three-quarter chord-line and midway span-wise. These collocation points are the points where the influence due to these vortices will be calculated. We also define the time step and path properties like initial velocity and change in pitch and plunge in the input file. The vortex ring coordinate points and collocation points are defined in body fixed reference frame. Figure 4.2 shows the three dimensional discrete vortex lattice model. The corresponding normal vectors for each panels are calculated using the the four coordinate points of the vortex ring as shown in the equation 4.3:

$$\vec{n} = \frac{\vec{A} \times \vec{B}}{\mid \vec{A} \times \vec{B} \mid} \tag{4.3}$$

where $\vec{A}$ and $\vec{B}$ are the vectors joining opposite corners of the vortex ring.

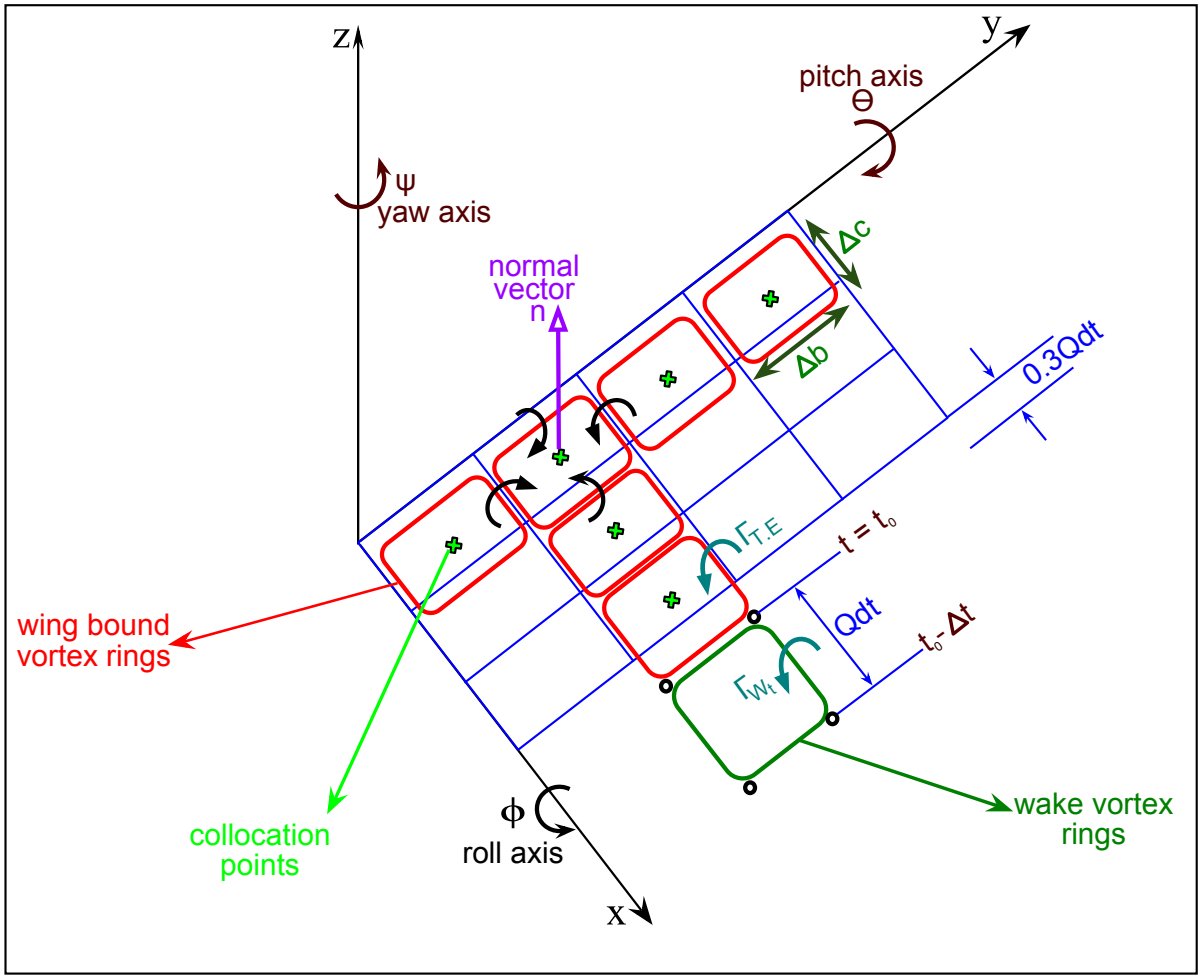

Figure 4.2: Unsteady Vortex Lattice Discretization Scheme

4.2.2 Self-Induced Influence Coefficients

The self-induced influence coefficients are the induced velocity components due to one ring's unit strength segments on the collocation points of another ring. To take into account the influence of every vortex ring on every collocation point, a single counter that counts all the rings on the wing was defined. The counter moves from left to right starting from leading edge panels moving chord-wise downwards. The Biot Savart's Law for induced velocity due to a line segment defined in above section is then used to calculate the influence of each segment of the

ring and then added up. However, as we have three dimensional coordinate points, the influence will have three components. Thus, to calculate the combined influence, we will dot product the total induced velocity vectors with the normal vector on the collocation points. The self induced influence coefficient matrix is given by,

$$[IC]_b = \begin{bmatrix} A_{11} & A_{12} & \dots & A_{1N} \\ A_{21} & A_{22} & \dots & A_{2N} \\ \vdots & \vdots & \ddots & \vdots \\ A_{N1} & A_{N2} & \dots & A_{NN} \end{bmatrix} \tag{4.4}$$

$$[u, v, w]_{ij} = [u_{b_1}, v_{b_1}, w_{b_1}]_{ij} + [u_{t_1}, v_{t_1}, w_{t_1}]_{ij} + [u_{b_2}, v_{b_2}, w_{b_2}]_{ij} + [u_{t_2}, v_{t_2}, w_{t_2}]_{ij} \tag{4.5}$$

where $A_{ij} = [u, v, w]_{ij} \cdot \hat{n}_i$ and $[u, v, w]_{ij}$ are components of the influence at the i^{th} bound vortex ring's collocation point due to all the vortex elements of j^{th} bound vortex ring and n_i is normal vector at the i^{th} bound vortex ring's collocation point. And b_1, t_1, b_2, t_2 are the four vortex elements of the j^{th} bound vortex ring.

4.2.3 Kinematics

The kinematics of the method follows the similar pattern from two dimensional method with an additional two degrees of freedom. We once again define two reference frames: one attached to the body and the other in the inertial reference frame. The transformation between these two frames is defined according to the order of rotation of the three axes. For instance, if we chose the order of rotation as $z-y-x$ i.e. yaw-pitch-roll the time-dependent kinematic velocity

due to transformation becomes,

$$\begin{pmatrix} U(t) \\ V(t) \\ W(t) \end{pmatrix} = \begin{pmatrix} \cos\psi(t) & \sin\psi(t) & 0 \\ -\sin\psi(t) & \cos\psi(t) & 0 \\ 0 & 0 & 1 \end{pmatrix} \begin{pmatrix} \cos\alpha(t) & 0 & -\sin\alpha(t) \\ 0 & 1 & 0 \\ \sin\alpha(t) & 0 & \cos\alpha(t) \end{pmatrix} \begin{pmatrix} 1 & 0 & 0 \\ 0 & \cos\phi(t) & \sin\phi(t) \\ 0 & -\sin\phi(t) & \cos\phi(t) \end{pmatrix} \begin{pmatrix} U_\infty \\ V_\infty \\ W_\infty \end{pmatrix} + \begin{pmatrix} -qz + ry \\ -rx + pz \\ -py + qx - \frac{\partial\eta}{\partial t} \end{pmatrix} \quad (4.6)$$

where $p = \dot{\phi}(t), q = \dot{\alpha}(t), r = \dot{\psi}(t)$ and x, y, z are the corresponding axis-wise distance of the coordinates of collocation points from the pivot point i.e. origin of the body fixed reference frame and $\frac{\partial\eta}{\partial t}$ is the wing's surface function for the non-flat-plate wings.

4.2.4 Wake Vortex Rings

The wake for the wing is also defined in the form of vortex rings. At each time step wake vortex ring corner points are created using the aft corner points of the trailing edge vortex rings, such that at first time step only two points of the wake vortex ring are formed. This suggests that at first time step there are no wake vortex rings and in the next time step using another set of aft corner points of the trailing edge that has advanced due to the translation, and the points from first time step wake vortex ring is created. This shedding procedure continues at each time step and a new set of wake vortex rings is formed. This shedding procedure is named as wake shedding procedure.

The strength of these wake vortex rings is set equal to the strength of the trailing edge vortex rings from the previous time step:

$$\Gamma_{W_t} = \Gamma_{T.E_{t-\Delta t}}$$

This procedure is in accordance with Helmholtz theorem which states that:

"Once the wake vortex is shed, its strength is unchanged as it moves with the local velocity"

4.2.5 Boundary Conditions

The boundary condition of zero normal flow on the surface i.e. ($Q_{n_K}(t) = 0$)is implemented on all bound vortex rings at the collocation points. The zero normal flow velocity condition at i^{th} vortex ring's collocation point is given by,

$$A_{i1}\Gamma_1 + A_{i2}\Gamma_2 + \ldots + A_{iN}\Gamma_N + [U(t) + u_W(t), V(t) + v_W(t), W(t) + w_W(t)]_i \cdot \hat{n}_i = 0 \quad (4.7)$$

where $[u_w(t), v_w(t), w_w(t)]_i$ is the down-wash induced on the i^{th} vortex ring's collocation point due to all the wake vortex rings at each time step. At each time step the number of wake vortex rings is increased due to which the down-wash induced changes at each time step. The down-wash induced is calculated using the wake influence. Wake influence is computed with the help of Biot Savart's law on the collocation points of the bound vortex rings using these wake vortex rings with the known strength at each time step. This wake influence is then added with the local time-dependent kinematic velocity to calculate the right hand side vector (RHS). Now again due to the three dimensional behavior of the problem the combined RHS vector at each collocation point is calculated by carrying out the dot product of the RHS vector with the normal vector at that collocation point. This whole procedure of calculating momentary RHS vector is carried out in each time step with the help of the single counter that was defined in earlier section. The momentary RHS vector is given by,

$$RHS_i(t) = -[U(t) + u_W(t), V(t) + v_W(t), W(t) + w_W(t)]_i \cdot \hat{n}_i \quad (4.8)$$

4.2.6 Solution Matrix

The Circulation for each bound vortex ring at each time step is calculated by combining the boundary condition equation for each bound vortex ring in a matrix form given by,

$$\begin{bmatrix} A_{11} & A_{12} & \dots & A_{1N} \\ A_{21} & A_{22} & \dots & A_{2N} \\ \vdots & \vdots & \ddots & \vdots \\ A_{N1} & A_{N2} & \dots & A_{NN} \end{bmatrix} \begin{bmatrix} \Gamma_1(t) \\ \Gamma_2(t) \\ \vdots \\ \Gamma_N(t) \end{bmatrix} = \begin{bmatrix} RHS_1 \\ RHS_2 \\ \vdots \\ RHS_N \end{bmatrix} \tag{4.9}$$

Now using these circulation values at each time step we will be able to calculate the pressures and aerodynamic loads for each panel and finally for the full wing.

4.2.7 Pressures and Aerodynamic Loads

The circulation calculated at each time from previous section is then transformed in the original discretized form using two counters one span-wise and other chord-wise. The pressure difference on the wing panels is dependent on the circulation values of the panels. The circulation for the leading edge panels is equal to Γ_{ij} and for other panels it is equal is equal to $\Gamma_{ij} - \Gamma_{i-1,j}$. The pressure difference is then computed using the Bernoulli equation 2.19 and can be given by,

$$\begin{aligned} \Delta p_{ij}(t) = \rho \left\{ [U(t) + u_W(t), V(t) + v_W(t), W(t) + w_W(t)]_{ij} \cdot \hat{\tau}_i \frac{\Gamma_{ij} - \Gamma_{i-1,j}}{\Delta c_{ij}} \right\} \\ + \rho \left\{ [U(t) + u_W(t), V(t) + v_W(t), W(t) + w_W(t)]_{ij} \cdot \hat{\tau}_j \frac{\Gamma_{ij} - \Gamma_{i,j-1}}{\Delta b_{ij}} + \frac{\partial}{\partial t} \Gamma_{ij} \right\} \end{aligned} \tag{4.10}$$

where $\hat{\tau}_i$ and $\hat{\tau}_j$ are the panel tangential vectors in the chord-wise and span-wise directions and Δc_{ij} and Δb_{ij} are the panel lengths in the chord-wise and span-wise directions The total normal force over the wing is then computed as,

$$F_N(t) = \sum_{i=1}^{L} \sum_{j=1}^{M} \Delta p_{ij}(t) \Delta S_{ij} \tag{4.11}$$

and non-dimensional normal force is then given by,

$$C_N(t) = \frac{F_N(t)}{(0.5\rho U^2 c)} \tag{4.12}$$

The leading edge suction force can also be computed by using the new approach discussed in the second chapter for two dimensional numerical method in equations from 2.24 to 2.31 . The LESP is calculated in the similar fashion an in equation 2.30 averaged over each span-wise panel and then added to get a combined LESP for full wing in order to compute the total three dimensional suction force. The non-dimensional leading edge suction force is given by following equation:

$$C_S(t) = \int_1^M \frac{2\pi A_0^2 dy}{S} \tag{4.13}$$

where M is the span-wise number of panels.

These two forces then contribute to the total lift and the drag of the wing. By using equations 4.12 and 4.13 the total non dimensional lift is then evaluated as,

$$C_L(t) = C_N(t)\cos\alpha\,(t) + C_S\,(t)\sin\alpha\,(t) \tag{4.14}$$

There is one extra component for the total drag of the wing and that is induced drag which is due to the induced down-wash W_{ind}, wake velocity w_W and the fluid acceleration. The induced down-wash is calculated using the circulations values at each panel and a secondary self-induced influence coefficient matrix which only has the vortex components that are parallel to the fluid direction, in other words the influence of only trailing vortex elements of the wing-bound vortex

rings. The secondary self-induced influence coefficient matrix is shown as,

$$[IC]_b^* = \begin{bmatrix} B_{11} & B_{12} & \dots & B_{1N} \\ B_{21} & B_{22} & \dots & B_{2N} \\ \vdots & \vdots & \ddots & \vdots \\ B_{N1} & B_{N2} & \dots & B_{NN} \end{bmatrix} \tag{4.15}$$

And the induced down-wash W_{ind} for each panel is then given by,

$$\begin{bmatrix} W_{ind-1} \\ W_{ind-2} \\ \vdots \\ W_{ind-N} \end{bmatrix} = \begin{bmatrix} B_{11} & B_{12} & \dots & B_{1N} \\ B_{21} & B_{22} & \dots & B_{2N} \\ \vdots & \vdots & \ddots & \vdots \\ B_{N1} & B_{N2} & \dots & B_{NN} \end{bmatrix} \begin{bmatrix} \Gamma_1 \\ \Gamma_2 \\ \vdots \\ \Gamma_N \end{bmatrix} \tag{4.16}$$

The induced drag can be calculated now using the following equation,

$$(\Delta D_{ind})_{ij} = \rho \left\{ (W_{ind} + w_W)_{ij} (\Gamma_{ij} - \Gamma_{i-1,j}) \Delta b_{ij} + \frac{\partial}{\partial t} \Gamma_{ij} \Delta S_{ij} \sin \alpha_{ij} \right\} \tag{4.17}$$

and the total drag is then calculated using the equations 4.12 , 4.13 and 4.17 given as,

$$C_D(t) = C_N(t) \sin \alpha\,(t) - C_S\,(t) \cos \alpha\,(t) + C_{D_{ind}} \tag{4.18}$$

Chapter 5

Results from the Three-Dimensional Analysis Method

The 3D numerical method is tested for some steady and unsteady cases. For the steady cases the results from numerical method are validated against the results from Weissinger's simplified vortex lattice method and Athena Vortex Lattice(AVL) program written by Drela and Youngren [42]. For unsteady cases the numerical method is validated against the results from the UVLM formulation given by Katz and Plotkin [40].

5.1 Validation of method using steady state results from Athena Vortex Lattice and Weissinger's Method

The validation is carried out by calculating the lift coefficient from three dimensional numerical method for five steady state cases of constant angle of attack of 5^o and each having different aspect ratios. The wing is divided into 52 panels, 4 chordwise and 13 spanwise divisions. The results are then compared with the values obtained from AVL and Weissinger's simplified vortex lattice method keeping the panel density the same.

AVL is a program for the aerodynamic and flight-dynamic analysis of rigid aircraft of arbi-

Table 5.1: Lift coefficient comparison between numerical method and AVL

Aspect Ratio	Numerical Method	AVL
4	0.3248	0.3224
8	0.4120	0.4082
12	0.4506	0.4463
20	0.4865	0.4820
200	0.5409	0.5405

trary configuration. It uses a extended version of vortex lattice method for calculations of forces on the lifting surfaces along with slender body model for fuselages and nacelles. The comparison of lift coefficient between numerical method and AVL is shown in table 5.1. We can evaluate from the results that both method are in congruence.

Weissinger's Method is a simplified vortex lattice method. In this method the wing is divided into panels only in spanwise direction, 13 panels on each side. Horseshoe vortices are placed on each panel by placing the bound vortex at the quarter chord line and collocation point at the three quarter chord line of the panel. Then the coefficients of the forces are calculated. The comparison of lift coefficients between Weissinger's method and the numerical method is shown in table 5.2. The comparison shows that the results from the numerical method compare well with those from AVL and Weissinger's method.

Table 5.2: Lift coefficient comparison between numerical method and Weissinger's Method

Aspect Ratio	Numerical Method	Weissinger's Method
4	0.3248	0.3196
8	0.4120	0.4067
12	0.4506	0.4455
20	0.4865	0.4817
200	0.5409	0.5405

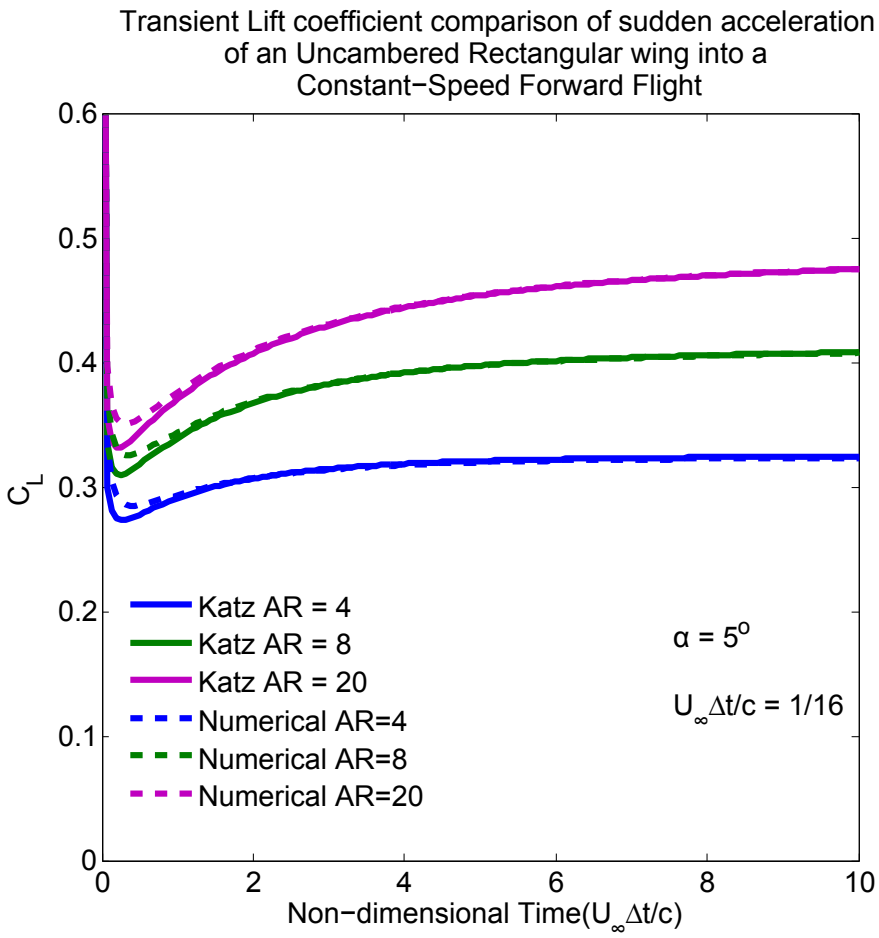

Figure 5.1: Transient lift coefficient comparison between the numerical method and digitalized results from Ref. [1] for abruptly started uncambered, rectangular wings

5.2 Validation for unsteady motions

The numerical method is validated against the results from the Ref. [1] for two cases, (1) the uncambered rectangular wing which is abruptly set into constant velocity motion and (2) the uncambered rectangular wing in heaving oscillatory motion. For the first case, three rectangular wings of aspect ratios as 4, 8 and 20 are abruptly set into constant velocity of 50 chord lengths per second in the direction of negative x direction. All wings are set at a constant angle of attack of 5^o. The numerical investigation is carried out using non-dimensional timestep of

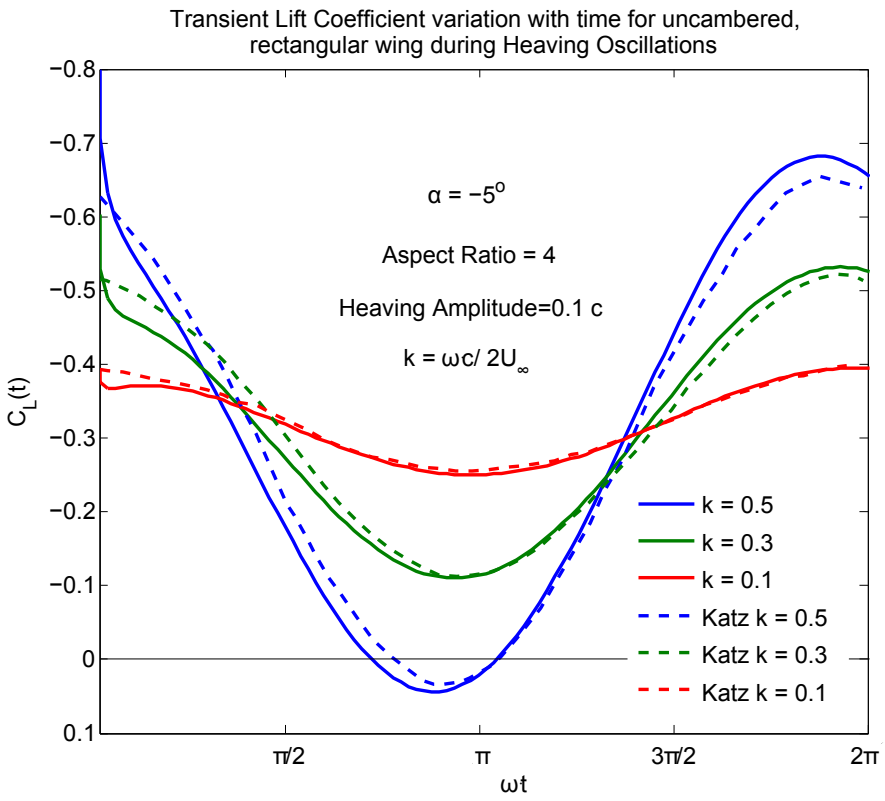

Figure 5.2: Transient lift coefficient comparison between the numerical method and digitalized results from Ref. [1] for heaving oscillations of uncambered, rectangular wing

$U_\infty \Delta t/c = 1/16$ and the wing divided into four chordwise and thirteen spanwise equally spaced panels. Figure 5.1 shows that the numerical method is producing overall a very good match with the results of Ref. [40]. The numerical method is over-predicting lift coefficient for some starting time-steps for case 1 but after that the results are in congruence.

For the second case a rectangular wing of aspect ratio of 4 is used. The wing is tested for heaving oscillations with three different frequency, ω = 10, 30, and 50. Heaving amplitude is kept constant as 10 percent of the chord length and the angle of attack for the wing as -5^o. The time step is taken as $\omega \cdot \Delta t$ where $\Delta t = c/(16U_\infty)$. Figure 5.2 shows that the numerical method is giving a very good estimate for the low frequency cases but for higher frequency cases a small discrepancy is observed.

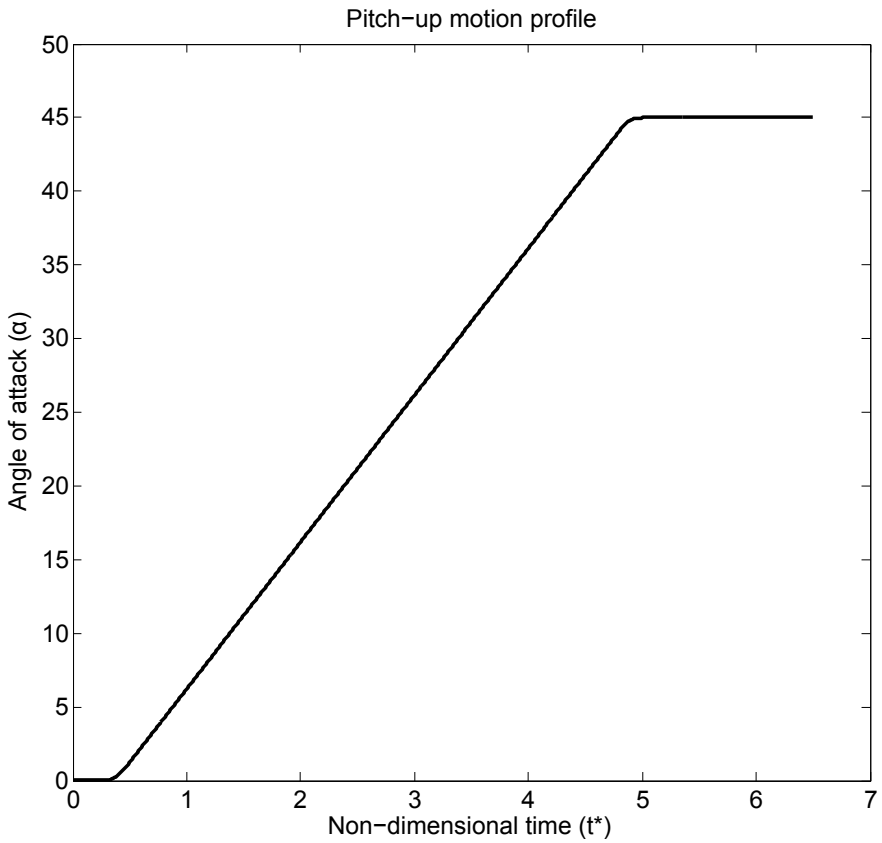

Figure 5.3: Pitch-up motion similar to that from Ref. [2] for 3D analysis on uncambered, rectangular wings

5.3 Extension of the LESP criterion to 3D wing analysis

The critical value of LESP calculated from the 2D analysis for an airfoil at a Reynolds number irrespective of motion kinematics is used to extend the LESP criterion to 3D analysis. A linear pitch-up motion about two pivot locations of the rectangular wing of aspect ratio = 2, from an angle of attack $\alpha = 0$ to 45^o is analyzed using the 3D method. The prescribed motion was rounded using the smoothing function developed by Eldredge et al. [43]. The pitch occurred over a dimensionless time scale $tU_\infty/c = 4$, represented by t^*. The pitch-ramp rate used is $\dot{\alpha}$ = 0.174 rad/s and the reduced pitch rate, based on chord c, is $K = \dot{\alpha}c/2U_\infty = 0.098$. The

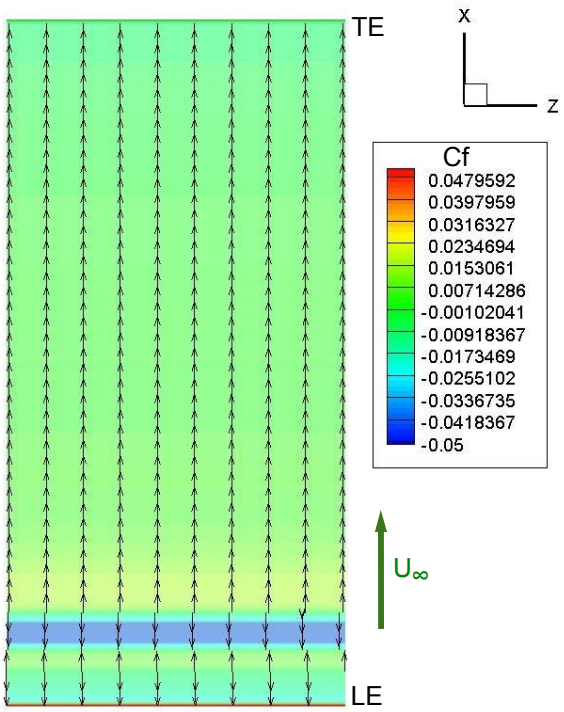

Figure 5.4: Case I, Quarter-chord pivot: Onset of LEV formation from preliminary CFD analysis on 2D flat plate at $\alpha = 8.21^o$. Flow is from bottom to top. [Courtesy of Dr. Edwards and Mr. Minao Shen]

freestream velocity was maintained at 90 mm/s and the corresponding Reynolds number based on root chord $c = 101.6$ mm, was 10000. Figure 5.3 shows the motion profile.

5.3.1 Case I :- Quarter-chord pivot location

From the 2D computational analysis carried out by Dr. Edwards CFD research group at NCSU of a flat plate for the linear pitch-up motion about the quarter chord pivot location is used to determine the critical LESP value. We observed from the 2D analysis that at $t = 1.202sec$ and $\alpha = 8.21^o$, the LEV starts forming and the critical LESP value from 2D numerical method for 50 panels discretization at this angle of attack is calculated as 0.09846.The contour plot with the streamlines for skin friction coefficient, C_f for the flat plate at the onset of LEV formation is shown in Figure 5.4. Here the first occurrence of a small region of positive C_f

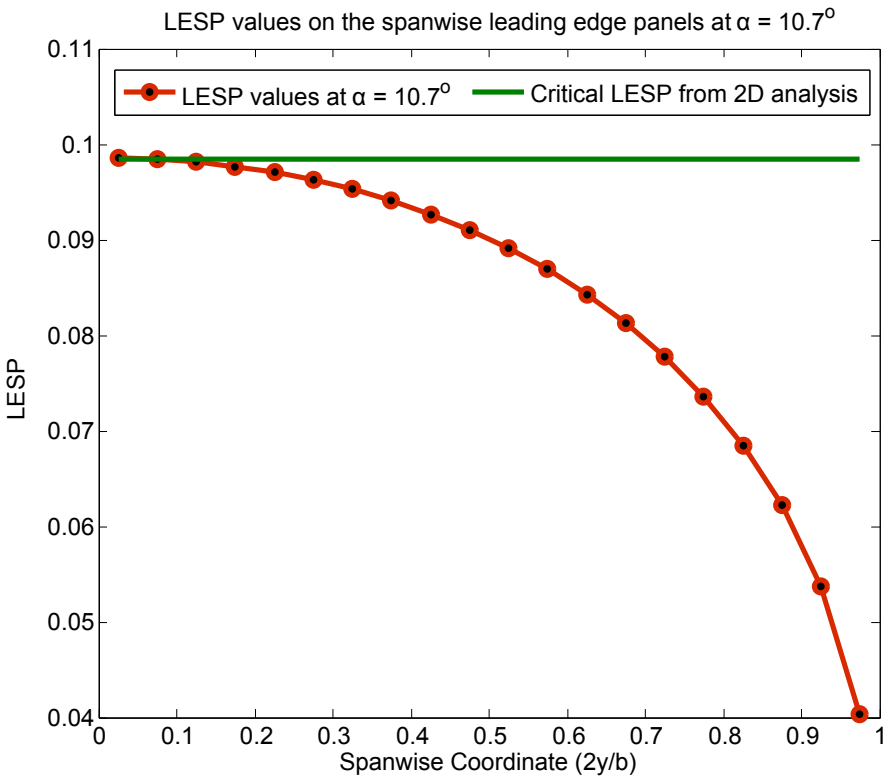

Figure 5.5: Case I, Quarter-chord pivot: Numerical method analysis on 3D rectangular wing representing the spanwise leading panels' LESP at $\alpha = 10.7^o$.

within the region of negative C_f is assumed to represent the onset of LEV formation. This way of determining the onset of LEV formation is adapted from Ramesh et. al. [27] A 3D numerical method analysis is carried out using 50 chordwise and 40 spanwise panels. According to the 3D numerical analysis, the onset of LEV is predicted to occur at an angle of attack of 10.7^o on the root near leading edge of the wing as the LESP of the panel near to the root from spanwise leading edge panels crosses the critical LESP value of 0.09846 (from 2D analysis) at this angle of attack, shown in Figure 5.5. The flat plate is used as cross-section for 3D computational analysis carried out on an unswept rectangular wing of aspect ratio 2. The results from the computational analysis carried out by Dr. Edward's CFD research group is used to verify the prediction criteria evaluated from the three-dimensional low-order numerical method. The LEV

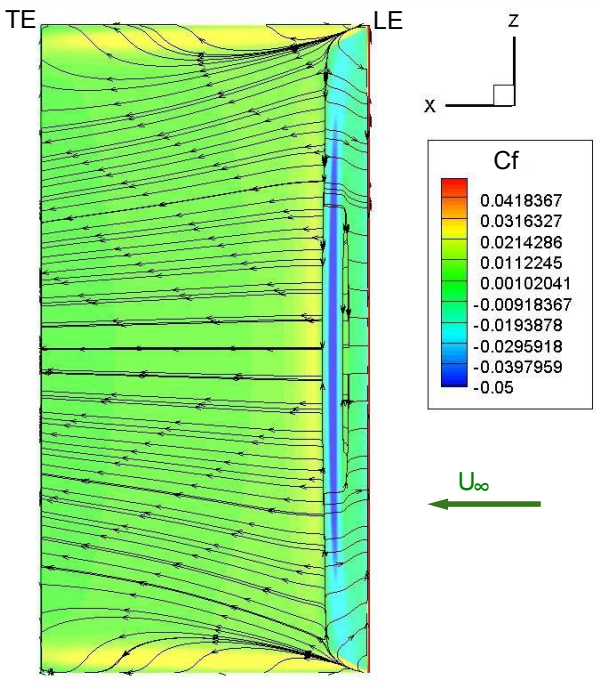

Figure 5.6: Case I, Quarter-chord pivot: Onset of LEV formation preliminary from CFD analysis on 3D rectangular wing at $\alpha = 9.71^o$. Flow is from right to left. [Courtesy of Dr. Edwards and Mr. Minao Shen]

formation occurs in three stages: (1) start of the flow separation at leading edge, (2) start of formation of the shear layer, and (3) establishment of the shear layer and the start of LEV shedding. The contour plots with streamlines for surface friction coefficient for 3D analysis is shown in Figure 5.6, representing the first occurrence of positive C_f on the root near leading edge of the wing at $\alpha = 9.71^o$.

The comparison between the values of the prediction criterion from computations and the numerical method is carried out and we found that there is a small discrepancy between the results. The low-order method is predicting the onset one degree of angle of attack later than the high-order computations, but both are predicting that the onset occurs near the root of the wing in the leading edge region.

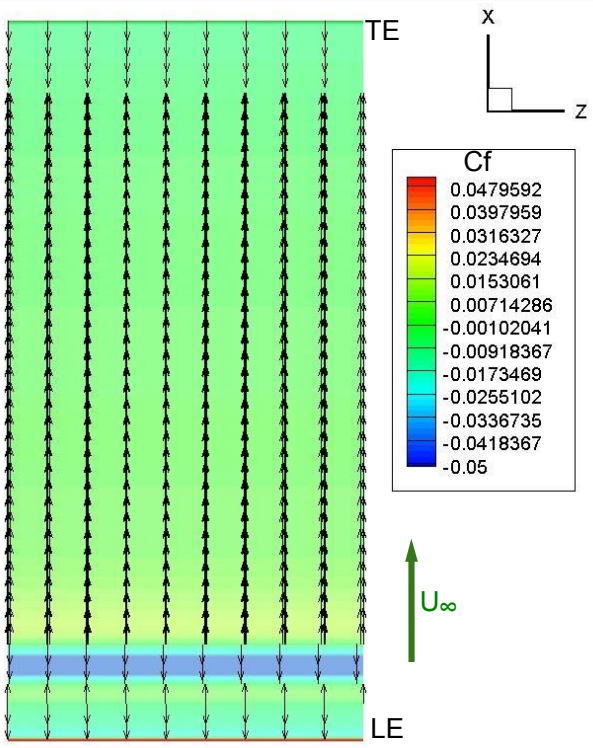

Figure 5.7: Case II, Three quarter-chord pivot: Onset of LEV formation from preliminary CFD analysis on 2D flat plate at $\alpha = 13.45^o$.Flow is from bottom to top. [Courtesy of Dr. Edwards and Mr. Minao Shen]

5.3.2 Case II :- Three quarter-chord pivot location

From the 2D computational analysis of a flat plate for the linear pitch-up motion about the three quarter chord pivot location we observed that at $t = 1.724sec$ and $\alpha = 13.45^o$, the LEV starts forming and the critical LESP value from 2D numerical method for 50 panels discretization at this angle of attack is calculated as 0.09519. This critical LESP value is nearly identical to that obtained for the 2D analysis in case I, confirming that LESP is independent of motion kinematics. The contour plot with the streamlines for C_f for the flat plate at the onset of LEV formation is shown in Figure 5.7. A 3D numerical method analysis is carried out using same number of panels as in case I. According to the 3D numerical analysis, the onset of LEV is predicted to occur at an angle of attack of 16.1^o on the root near leading edge of the wing as

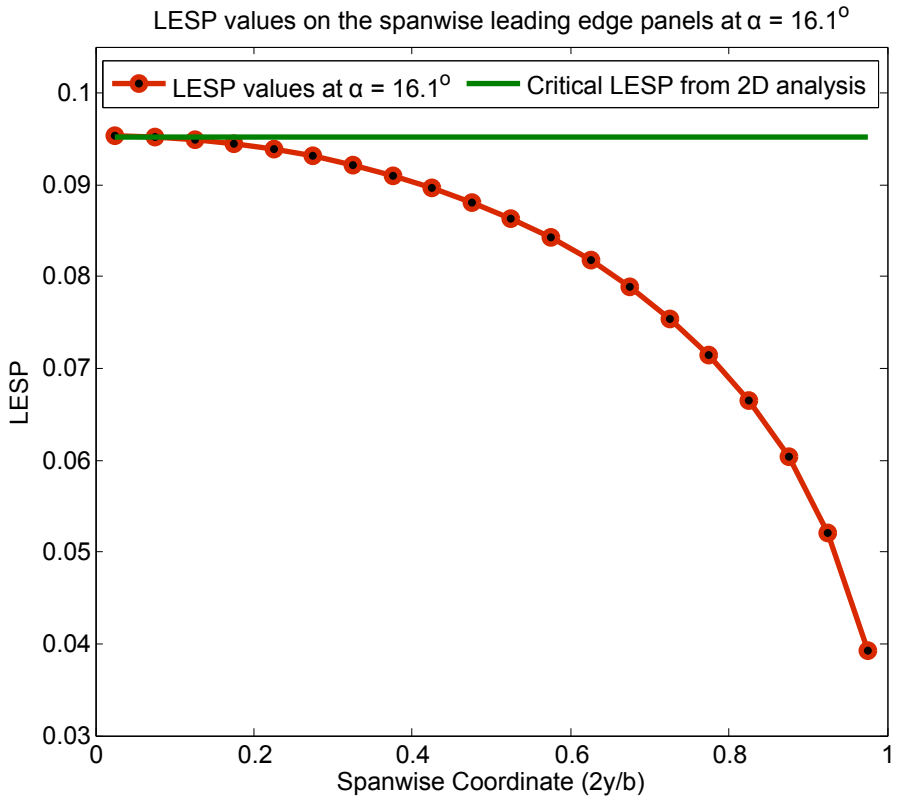

Figure 5.8: Case II, Three quarter-chord pivot: Numerical method analysis on 3D rectangular wing representing the spanwise leading panels' LESP at $\alpha = 16.1^o$.

the LESP of the panel near to the root from spanwise leading edge panels crosses the critical LESP value of 0.09519 (from 2D analysis) at this angle of attack, shown in Figure 5.8. The contour plots with streamlines for surface friction coefficient for 3D computational analysis is shown in Figure 5.9, representing the onset of LEV formation on the root near leading edge of the wing at $\alpha = 15.09^o$.

The comparison between the values of the prediction criterion from computations and the numerical method is carried out and we found that there is a small discrepancy between the results. The low-order method is predicting the onset one degree of angle of attack later than the high-order computations, but both are predicting that the onset occurs near the root of the wing in the leading edge region.

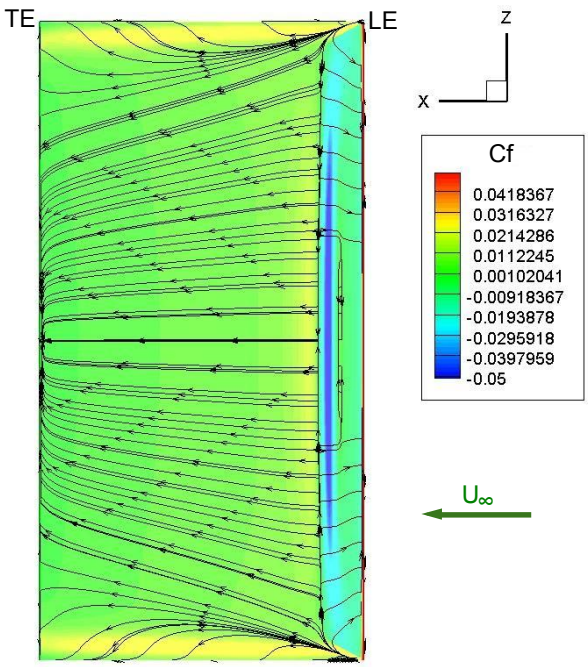

Figure 5.9: Case II, Three quarter-chord pivot: Onset of LEV formation preliminary from CFD analysis on 3D rectangular wing at $\alpha = 15.09^o$.Flow is from right to left. [Courtesy of Dr. Edwards and Mr. Minao Shen]

5.4 Discussion

The observation from the results and comparisons is that the numerical method is working nicely and approximately predicting the onset of LEV formation. The numerical method needs to include a LEV model for correctly predicting LEV shedding and its effects for LEV dominated motions. The numerical method is able to predict the correct position of start of LEV formation but needs further work in order to correct the discrepancy observed in the value of angle of attack of onset.

Chapter 6

Conclusions

Unsteady aerodynamic phenomena are becoming increasingly important in modern aerospace applications as we aim to develop micro air vehicles and improve the performance of wind turbines and rotorcraft. There are some effects induced by unsteady flows that elude our understanding for design and control, including dynamic stall in rotor dynamics, LEV formation and flow separation. These effects make a huge influence on performance in rotorcraft and animal flight. In past few decades advancement in computations and experiments have enriched us with the knowledge of these effects, albeit at significant computational time and costs which is not available in the early design stages. These high computational costs motivate the development of low-order methods. Unfortunately reliable low-order methods for 3D wings that can predict and control the "start" and "stop" of these unsteady effects is not yet available. In this research, we have developed a low-order numerical methodology for 2D and 3D unsteady flow problems. The objective is to determine the onset criterion for LEV shedding.

A numerical method based on 2D discrete vortex element distribution on airfoil and capable of handling large amplitude kinematics and non-planar wakes is developed to predict the onset of the LEV formation using a critical value of parameter similar to LESP. The forward-most bound vortex of the airfoil is found to have a behavior similar to the LESP in theoretical method. A parameter similar to LESP based on the strength of the forward-most bound vortex

is introduced. The motivation for this research comes from the desire to replace the Fourier-series based theoretical method which cannot be extended to 3D analysis of finite wings. The validity of the two-dimensional numerical method is checked using the results from the theoretical method, experiments and computations. As expected this numerical method produces the same amount of accuracy as of the theoretical method until the flow is dominated by LEVs. The LESP is able to provide us with the critical point that represents the onset of LEV formation for a particular airfoil at certain Reynolds number irrespective of the motion kinematics. This critical value of LESP is determined using information from computations or experiments.

An extension of this LESP criterion to three dimensional wing and rotor analysis is developed. This extension is based on unsteady vortex lattice formulation that in itself is an extension of the two-dimensional discrete vortex method. The objective is to find the critical time instant in a motion at which the LEV formation will start. In this three-dimensional numerical method the vortex strength of the forward-most panel on the wing is used to determine the LESP variation along the span. The position and criterion of onset on unswept three-dimensional wing for any given motion kinematics is calculated using the predetermined critical value of LESP from two-dimensional analysis for an airfoil and Reynolds number. The validation of the three-dimensional numerical method is done for some steady and unsteady motions. Results from these comparisons proves that this inviscid numerical method shows promise in the prediction of onset of LEV formation on 3D wings.

This research serves as a stepping stone towards the greater objective of being able to be control the LEV formation according to the motion requirements. The future work includes the augmentation of this current method to account for the effects of fully developed LEV formation and shedding on the three-dimensional wings. At this stage we have the insight of onset criterion and the possible location of the LEV formation on the wing-span. Using this information an LEV model can be included in the method which will be very helpful in the prediction of LEV shedding and its effects.

REFERENCES

[1] Katz, J., "Calculation of the aerodynamics forces on automotive lifting surfaces," *Journal of Fluid Engineering*, Vol. 107, 1985, pp. 438–443.

[2] Yilmaz, T. and Rockwell, D., "Flow structure on finite-span wings due to pitch-up motion," *Journal of Fluid Mechanics*, Vol. 691, 2012, pp. 518–545.

[3] Dial, K. P., "An inside look at how birds fly: experimental studies of the internal and external processes controlling flight," *Report to the Aerospace Profession, 38th Symp Proc, The Beverly Hilton, Beverly Hills, CA*, 1994.

[4] Mueller, T. J., *Fixed and flapping wing aerodynamics for micro air vehicle applications*, Vol. 195, AIAA, 2001.

[5] Theodorsen, T., "General theory of aerodynamic instability and the mechanism of flutter," NACA Rept. 496, 1935.

[6] Wagner, H., "ber die Entstehung des dynamischen Auftriebes von Tragflgeln," *ZAMM - Journal of Applied Mathematics and Mechanics / Zeitschrift fr Angewandte Mathematik und Mechanik*, Vol. 5, No. 1, 1925, pp. 17–35.

[7] Garrick, I., "Propulsion of a flapping and oscillating airfoil," NACA TR No. 576, 1937.

[8] Garrick, I., "On some reciprocal relations in the theory of non-stationary flows," NACA TR No. 629, 1938.

[9] von Kármán, T. and Burgers, J. M., "General aerodynamic theory — perfect fluids," *Aerodynamic Theory: A General Review of Progress*, Vol. 2, Julius Springer, Berlin, Germany, 1935.

[10] Küssner, H., "Zusammenfassender Bericht über den instationären Auftrieb von Flügeln," *Luftfahrtforschung*, Vol. 13, No. 12, 1936, pp. 410–424.

[11] von Kármán, T. and Sears, W., "Airfoil theory for non-uniform motion," *Journal of the Aeronautical Sciences (Institute of the Aeronautical Sciences)*, Vol. 5, No. 10, 1938.

[12] Loewy, R. G., "A two-dimensional approximation to the unsteady aerodynamics of rotary wings," *Journal of the Aeronautical Sciences (Institute of the Aeronautical Sciences)*, Vol. 24, No. 2, 1957.

[13] Weis-Fogh, T., "Quick estimates of flight fitness in hovering animals, including novel mechanisms for lift production," *Journal of Experimental Biology*, Vol. 59, 1973.

[14] Maxworthy, T., "Experiments on the Weis-Fogh mechanism of lift generation by insects in hovering flight. Part 1. Dynamics of the fling," *Journal of Fluid Mechanics*, Vol. 93, 7 1979, pp. 47–63.

[15] van den Berg, C. and Ellington, C. P., "The vortex wake of a 'hovering' model hawk-moth," *Philosophical Transactions of the Royal Society of London. Series B: Biological Sciences*, Vol. 352, No. 1351, 1997, pp. 317–328.

[16] Ellington, C. P., Van Den Berg, C., Willmott, A. P., and Thomas, A. L., "Leading-edge vortices in insect flight," *Nature*, Vol. 384, 1996, pp. 626–630.

[17] Birch, J. M. and Dickinson, M. H., "Spanwise flow and the attachment of the leading-edge vortex on insect wings," *Nature*, Vol. 412, No. 6848, 2001, pp. 729–733.

[18] Birch, J. M., Dickson, W. B., and Dickinson, M. H., "Force production and flow structure of the leading edge vortex on flapping wings at high and low Reynolds numbers," *Journal of Experimental Biology*, Vol. 207, No. 7, 2004, pp. 1063–1072.

[19] Singh, B. and Chopra, I., "Insect-based hover-capable flapping wings for micro air vehicles: experiments and analysis," *AIAA Journal*, Vol. 46, No. 9, 2008, pp. 2115–2135.

[20] McCroskey, W., "The phenomenon of dynamic stall," Tech. rep., NASA TM 81264, 1981.

[21] Carr, L. W., "Progress in analysis and prediction of dynamic stall," *Journal of Aircraft*, Vol. 25, No. 1, 1988, pp. 6–17.

[22] Jones, K. D. and Platzer, M. F., "On the prediction of dynamic stall onset on airfoils in low speed flow," *Unsteady Aerodynamics and Aeroelasticity of Turbo-machines*, Springer, 1998, pp. 797–812.

[23] Geissler, W. and Haselmeyer, H., "Investigation of dynamic stall onset," *Aerospace Science and Technology*, Vol. 10, No. 7, 2006, pp. 590 – 600.

[24] Rival, D. E., Kriegseis, J., Schaub, P., Widmann, A., and Tropea, C., "A criterion for vortex separation on unsteady aerodynamic profiles," *AIAA Paper* 2013 − 0836, 2013.

[25] Nangia, R., "Semi-empirical prediction of vortex onset and progression on delta wings," *AIAA Paper* 2008 − 0384, 2008.

[26] Leishman, J. and Beddoes, T., "A semi-empirical model for dynamic stall," *Journal of the American Helicopter Society*, Vol. 34, No. 3, 1989, pp. 3–17.

[27] Ramesh, K., Gopalarathnam, A., Ol, M. V., Granlund, K., and Edwards, J. R., "Augmentation of inviscid airfoil theory to predict and model 2d unsteady vortex dominated flows," *AIAA Paper* 2011 − 3578, 2011.

[28] Belotserkovskii, S., "Study of the unsteady aerodynamics of lifting surfaces using the computer," *Annual Review of Fluid Mechanics*, Vol. 9, No. 1, 1977, pp. 469–494.

[29] Rogers, S. E., Kwak, D., and Kiris, C., "Steady and unsteady solutions of the incompressible Navier-Stokes equations," *AIAA Journal*, Vol. 29, No. 4, 1991, pp. 603–610.

[30] Visbal, M., Yilmaz, T. O., and Rockwell, D., "Three-dimensional vortex formation on a heaving low-aspect-ratio wing: computations and experiments," *Journal of Fluids and Structures*, 2013.

[31] De Young, J., "Optimum lattice arrangement developed from a rigorous analytical basis," *Vortex-Lattice Utilization*, Vol. 405, 1976, p. 343.

[32] Hedman, S. G., "Vortex lattice method for calculation of quasi steady state loadings on thin elastic wings in subsonic flow," Tech. rep., Aeronautical Research Institute of Sweden Stockholm, FFA - 105, 1966.

[33] Levin, D. and Katz, J., "Vortex-lattice method for the calculation of the nonsteady separated flow over delta wings," *Journal of Aircraft*, Vol. 18, No. 12, 1981, pp. 1032–1037.

[34] Konstadinopoulos, P., Thrasher, D., Mook, D., Nayfeh, A., and Watson, L., "A vortex-lattice method for general, unsteady aerodynamics," *Journal of Aircraft*, Vol. 22, No. 1, 1985, pp. 43–49.

[35] Long, L. N. and Fritz, T. E., "Object-oriented unsteady vortex lattice method for flapping flight," *Journal of Aircraft*, Vol. 41, No. 6, 2004, pp. 1275–1290.

[36] Mook, D. and Maddox, S., "Extension of a vortex-lattice method to include the effects of leading-edge separation," *Journal of Aircraft*, Vol. 11, No. 2, 1974, pp. 127–128.

[37] Murua, J., Palacios, R., and Graham, J. M. R., "Applications of the unsteady vortex-lattice method in aircraft aeroelasticity and flight dynamics," *Progress in Aerospace Sciences*, 2012.

[38] Smith, M., Wilkin, P., and Williams, M., "The advantages of an unsteady panel method in modeling the aerodynamic forces on rigid flapping wings," *Journal of Experimental Biology*, Vol. 199, No. 5, 1996, pp. 1073–1083.

[39] Mata Bueso, E., *Unsteady aerodynamic vortex lattice of moving aircraft*, Master's thesis, KTH, Aerodynamics, 2011.

[40] Katz, J. and Plotkin, A., *Low Speed Aerodynamics From Wing Theory to Panel Methods*, McGraw-Hill,Inc., New York, 1991.

[41] Ramesh, K., Gopalarathnam, A., Edwards, J., Ol, M., and Granlund, K., "An unsteady airfoil theory applied to pitching motions validated against experiment and computation," *Theoretical and Computational Fluid Dynamics*, 2013, pp. 1–22.

[42] Drela, M. and Youngren, H., "Athena vortex lattice user manual, Version 3.26," 2006.

[43] Eldredge, J. D., Wang, C., and Ol, M., "A computational study of a canonical pitch-up, pitch-down wing maneuver," *AIAA Paper* 2009 − 3687, 2009.

[44] Cassidy, D. A., Edwards, J. R., and Tian, M., "An investigation of interface-sharpening schemes for multi-phase mixture flows," *Journal of Computational Physics*, Vol. 228, No. 16, 2009, pp. 5628 – 5649.

[45] Neaves, M. D. and Edwards, J. R., "All-speed time-accurate underwater projectile calculations using a preconditioning algorithm," *Journal of Fluids Engineering*, Vol. 128, No. 2, 2006, pp. 284–296.

[46] Choi, J.-I., Oberoi, R. C., Edwards, J. R., and Rosati, J. A., "An immersed boundary method for complex incompressible flows," *Journal of Computational Physics*, Vol. 224, No. 2, 2007, pp. 757–784.

[47] Ol, M. V., Bernal, L., Kang, C.-K., and Shyy, W., "Shallow and deep dynamic stall for flapping low Reynolds number airfoils," *Animal Locomotion*, Springer, 2010, pp. 321–339.

[48] Granlund, K., Ol, M., and Bernal, L., "Experiments on pitching plates: force and flow-field measurements at low Reynolds Numbers," *AIAA Paper* 2011 − 0872, 2011.